

SUPPORTING INFORMATION

FOR

Folding-Degradation Relationship of a Membrane Protein Mediated by the Universally Conserved ATP-dependent Protease FtsH

Yiqing Yang,^{†,||} Ruiqiong Guo,^{†,||} Kristen Gaffney,^{‡,||} Miyeon Kim,[†] Shaima Muhammednazaar,[†]
Wei Tian,[§] Boshen Wang,[§] Jie Liang,[§] and Heedeok Hong^{*,†,‡}

[†]Department of Chemistry and [‡]Department of Biochemistry & Molecular Biology, Michigan State University, East Lansing, Michigan 48824, United States

[§]Department of Bioengineering, University of Illinois at Chicago, Chicago, Illinois 60607, United States

^{||}These authors contributed equally to this work.

*Correspondence: honghd@msu.edu

Tel: 1-517-353-1104

CONTENTS

SUPPORTING METHODS (p.S3–S11)

SUPPORTING TABLES (p.S12–S15)

Table S1. Kinetic parameters of ATPase activity of FtsH in various lipid environments.

Table S2. Folding parameters of water-soluble model substrates and GlpG for AAA+ proteases.

Table S3. Kinetic parameters of GlpG degradation by FtsH.

Table S4. $\Delta G_{\text{dislocation}}$ of individual TM helices of GlpG using membrane-depth dependent transfer free energy.

Table S5. The effects of bound substrates on ATPase activity of FtsH.

Table S6. Comparison of ATP costs during degradation of several proteins by AAA+ proteases.

SUPPORTING FIGURES (p.S16–S32)

Figure S1. ATPase activity of FtsH as model degradation machinery.

Figure S2. Thermostability of GlpG in various lipid environments.

Figure S3. Time-dependent degradation of GlpG variants *in vivo*.

Figure S4. FtsH-mediated degradation of GlpG in bicelles.

Figure S5. Steric trapping of GlpG to measure the spontaneous unfolding rate k_U .

Figure S6. Unfolding energy landscape of GlpG in DDM micelles revealed by steric trapping.

Figure S7. Characterization of M100A and LLWF variants.

Figure S8. Calculation of the free energy of dislocation ($\Delta G_{\text{dislocation}}$) using the depth-dependent hydrophobicity scale.

Figure S9. ATPase activity of FtsH in the presence of bound substrate.

Figure S10. A mechanical model to explain why FtsH more efficiently degrades membrane proteins than water-soluble proteins.

REFERENCES FOR SUPPORTING INFORMATION (p.S33–35)

SUPPORTING METHODS

Cloning, expression and purification of FtsH. The coding region for full-length FtsH was PCR-amplified from genomic DNA of the *E. coli* strain MG1655 and subcloned into pET21a expression vector encoding C-terminal His₆-tag.

For FtsH expression, *E. coli* C43 (DE3) pLysS cells containing plasmids encoding FtsH were grown on selection plates (100 mg/L ampicillin) at 37°C. A liquid culture was inoculated with a single colony and grown in LB media (100 mg/L ampicillin) overnight at 37°C until the cells reach the stationary phase. The overnight culture was used to inoculate a fresh LB media (100 mg/L ampicillin) and cultivated to the mid-exponential phase (OD_{600nm} = 1.2) at 37°C. The culture was induced with 1 mM isopropyl β-D-thiogalactopyranoside (IPTG) and was grown at 37°C for an additional 3 h.

Harvested cells were resuspended in 1/40 culture volume of resuspension buffer of 25 mM Tris-HCl (pH 8.0), 0.1% β-mercaptoethanol (BME) (v/v), 15% glycerol (v/v) and 0.5 mM phenylmethylsulfonyl fluoride (PMSF). Cells were lysed five times using EmulsiFlex-C5 pressure homogenizer (Avestin). After removal of cell debris by centrifugation in F21 rotor using a Sorvall RC6+ centrifuge (Thermo Fisher Scientific) at 6,000 rpm for 30 min, the total membrane fraction was obtained by ultracentrifugation (Beckman Coulter, Type 45 Ti rotor) at 28,000 rpm for 2 h. The total membrane pellets were resuspended in 1/50 culture volume Base Buffer (25 mM Tris-HCl pH 8.0, 200 mM KCl, 15% glycerol) using tissue homogenizer. The membrane resuspension was solubilized by addition of Triton X-100 to a final concentration of 2% (w/v). Aggregation was removed by centrifugation at 12,000 rpm for 1 h. FtsH was purified from resulting supernatant using Ni²⁺-NTA affinity chromatography (Qiagen, 1 mL resin volume per liter culture). After washing the resin with 10-resin volume of wash buffer (Base Buffer with 0.1% Triton X-100, 20 mM imidazole), bound FtsH was eluted with 10-resin volume of Elution Buffer (Base Buffer with 0.1% Triton X-100, 0.1% BME, 200 mM imidazole). Eluent was concentrated using a centrifugal filtration unit (Millipore, 50 kDa MWCO). After removal of excess imidazole in a desalting column (Bio-Rad) equilibrated with Base Buffer with 0.1% Triton X-100 and 0.1% BME, FtsH was concentrated to the final volume of 0.5~1.0 mL per 1 liter culture (typically, 60~150 μM). All purification procedures were carried out at 4°C. The protein concentration was determined by 660 nm protein assay (Bio-Rad) which was compatible with Triton X-100.

ATPase Activity Assay of FtsH. ATP hydrolysis rate by FtsH was measured by an enzyme-coupled assay. The assay mixture (typically 100 μL) in a 96-well UV-compatible microplate (Greiner Bio-One) contained 2 μM FtsH, 20 mM HEPES (pH 7.8), 10 mM MgCl₂, 400 μM ZnCl₂, 0.1% BME, 100 mM KCl, 15% glycerol, 0.5 mM NADH, 10 mM phosphoenolpyruvic acid, 0.5 units of pyruvate kinase and 0.5 units of lactic dehydrogenase. The oxidation of NADH coupled to ATP hydrolysis was monitored at 37°C by continuous monitoring absorbance at 340 nm on a microplate reader (M5e, Molecular Devices). Data analysis and fitting equations to calculate ATP hydrolysis rate (v_{ATP}) by FtsH hexamer per minute are shown as following:

$$v_{ATP} = \frac{\frac{\Delta Abs}{\min}}{\frac{\Delta Abs}{[ATP]}} \times \frac{1}{[FtsH_6]} \quad (\text{Equation 1})$$

A fitting equation using Michaelis-Menten kinetics for ATPase activity of FtsH is given as:

$$v_{\text{ATP}} = \frac{k_{\text{cat,ATP}}[\text{ATP}]}{K_{\text{m,ATP}} + [\text{ATP}]} \quad (\text{Equation 2})$$

, where v_{ATP} is ATP hydrolysis rate, $k_{\text{cat,ATP}}$ is a maximal ATP turnover number by FtsH hexamer per min, and $K_{\text{m,ATP}}$ is Michaelis constant, the ATP concentration at which ATP hydrolysis rate reaches the half-maximum.

Hill equation to fit ATPase activity of FtsH is given as:

$$v_{\text{ATP}} = \frac{[\text{ATP}]^{n_{\text{H,ATP}}}}{K_{\text{m,ATP}}^{n_{\text{H,ATP}}} + [\text{ATP}]^{n_{\text{H,ATP}}}} \quad (\text{Equation 3})$$

, where $n_{\text{H,ATP}}$ is Hill constant of FtsH hexamer ATPase activity.

Preparation of Bicelles. 15% (w/v) stock of DMPC (1,2-dimyristoyl-*sn*-glycero-3-phosphocholine)/DMPG (1,2-dimyristoyl-*sn*-glycero-3-phospho-(1'-*rac*-glycerol))/CHAPS (3-[(3-Cholamidopropyl)dimethylammonio]-1-propanesulfonate) (lipid-to-detergent molar ratio, $q = 2.8$) bicelles were prepared by hydrating DMPC/DMPG (molar ratio = 3:1) lipids with water. Sonication was applied if necessary. When homogeneous lipid suspension was formed, 20% (w/v) CHAPS was added to reach the desired q value. The mixture was then gently stirred at 4°C until the solution becomes completely clear. Bicelle samples were further homogenized through three cycles of freeze-thaw using liquid nitrogen and a water bath at 37°C. Prepared sample stocks were kept at -20°C prior to use. 15% (w/v) stock of DMPC/CHAPS ($q = 2.8$) bicelles were prepared in the same way as above.

Lipid and Protein Diffusion Assays in Bicelles. 3% (w/v) bicelles (DMPC/DMPG/CHAPS, $q = 2.8$) without fluorophores (hereafter, unlabeled bicelles) were prepared in 20 mM HEPES (pH 7.5), 15% glycerol (v/v), 80 mM KCl and 10 mM MgCl₂ buffer by diluting 15% bicelle stock solution described above. The bicelles containing fluorescently labeled lipids were prepared using the following procedures: First, DMPC and DMPG lipids (DMPC:DMPG molar ratio = 3:1) dissolved in chloroform were mixed with NBD (nitrobenzoxadiazole)-DPPE (1,2-dipalmitoyl-*sn*-glycero-3-phosphoethanolamine) (FRET donor) and Rh (rhodamine)-DPPE (FRET acceptor) lipids which were also dissolved in chloroform at a lipid mole fraction of 0.01 for each. The lipid solution was dried under a stream of nitrogen gas and further in vacuum for 2 h. The resultant lipid film was resuspended in 20 mM HEPES (pH 7.5), 15% glycerol, 80 mM KCl and 10 mM MgCl₂ buffer. Desired amount of CHAPS was added to a final lipid and detergent concentration of 3% (w/v) to form the fluorescent bicelles. Lipid diffusion in bicelles was tested by mixing the fluorescent bicelles with unlabeled bicelles at a 1:35 volume ratio and monitoring FRET signal, *i.e.*, the ratio of fluorescence intensity of NBD at 530 nm to that of Rh at 590 nm, as a function of time. As a negative control that represents no diffusion, the fluorescent bicelles were mixed with buffer solution. As a positive control that represents a homogeneously mixed state, the bicelles containing NBD-DPPE and the bicelles containing Rh-DPPE were added separately to unlabeled bicelles and carefully mixed.

Diffusion of protein components in bicelles was also tested to evaluate the time scale of the interaction between FtsH and substrates, both of which are integrated in bicelles. The principle is similar to that of the lipid diffusion assay described above. Instead of using fluorescently labeled

lipids, we incorporated the model membrane substrate GlpG labeled with NBD or Rh into DMPC/DMPG/CHAPS bicelles by direct injection of GlpG solubilized in *n*-dodecyl- β -D-maltoside (DDM, Anatrace) to bicelles. The fluorescent GlpG-bicelle complex contained 74 μ M of NBD-GlpG and 74 μ M of Rh-GlpG. GlpG diffusion in bicelles was tested by measuring the ratio of fluorescence intensity of NBD at 530 nm to that of Rh at 590 nm as a function of time. As a negative control that represents no diffusion of proteins, the bicelles containing NBD and Rh labeled GlpG were mixed with buffer solution without bicelles. As a positive control that represents a homogeneously mixed state, the bicelles containing NBD-GlpG and the bicelles containing Rh-GlpG were added separately to unlabeled bicelles without incorporated proteins. All fluorescence measurements were performed on PTI QW4 fluorimeter at 37°C with a final sample volume of 1,400 μ L. For FRET, the excitation wavelength for NBD was 467 nm, and the emission wavelengths were 530 nm for NBD and 590 nm for Rh. Both excitation and emission slit-widths were set to 0.75 nm.

Thermostability of GlpG in Lipid Environments. Thermostability of the model substrate GlpG was studied in bicelles, liposomes and micelles by measuring resistance to irreversible thermal inactivation and aggregation. To measure the thermostability in bicelles, GlpG-108 (see below for cloning, expression and purification of GlpG variants for detailed information) in DDM was incorporated into 2 mL of 3% (w/v) DMPC/DMPG/CHAPS bicelle solution (20 mM HEPES, 15% glycerol, 100 mM NaCl, pH 7.5 buffer) to a final concentration of 5 μ M by direct injection of concentrated GlpG-108 in DDM into preformed bicelles and incubating for 1h on ice. The total volume was transferred to a quartz cuvette and heated from 25°C to 90°C with a 5°C interval in the cuvette holder on CARY 100 Series UV-Vis spectrophotometer connected to a temperature-controller. At each target temperature, the sample was incubated for 5 min, and then 100 μ L sample was aliquoted from the cuvette and cooled down on ice for 1 h. 70 μ L from each aliquot was used for measuring thermal aggregation and 25 μ L for thermal inactivation. Thermal aggregation was measured by absorbance at 320 nm at room temperature. Thermal inactivation was measured by fluorescence-based GlpG activity assay,¹ which was carried out by addition of 25 μ L of SN-LacYTM2 labeled with NBD, the model GlpG substrate, to a final concentration of 10 μ M at room temperature (**Figure S2a**). The substrate was pre-incorporated in 3% bicelles.

To measure the thermostability in *E. coli* liposomes, GlpG-108 was first reconstituted in *E. coli* lipid vesicles. Dried *E. coli* lipid (Avanti Polar Lipids) film was hydrated with 20 mM HEPES (pH 7.5), 100 mM NaCl buffer to a final lipid concentration of 10 mM. The lipid suspension was homogenized by three cycles of freeze-thaw and then extruded through 0.2 μ M pore size polycarbonate membrane (Whatman). DDM was added to the liposome suspension to a final concentration of 10 mM and incubated for 30 min, and GlpG protein stock was added to a final concentration of 5 μ M. The lipid-protein-detergent mixture was incubated for 30 min. For detergent removal, three portions of Bio-Beads (Bio-Rad) were added (20 mg/mL for each) stepwise. In each step, the mixture was gently stirred for 1–2 h at room temperature. The resulting proteoliposomes were extruded again using 0.2 μ M pore size membrane. 2.0 mL of reconstituted GlpG in 20 mM HEPES (pH 7.5), 100 mM NaCl buffer at a concentration of 5 μ M was added to a quartz cuvette. Sample heating and aliquoting were performed in the same way as in bicelles. For the samples to measure irreversible aggregation, one portion from each aliquoted sample was solubilized with a final concentration of 2% (w/v) octyl- β -glucoside (β -OG, Anatrace) and incubated overnight, and absorbance at 320 nm was measured at room temperature. For the samples to measure irreversible inactivation, the other portion from the

aliquoted sample was solubilized in 20 mM DDM overnight and GlpG activity (1 μ M at a final concentration) was measured by addition of NBD-labeled SN-LacYTM2 in DDM to a final concentration of 10 μ M.

As a control, thermostability of GlpG-108 was measured in DDM under the same condition used by Baker and Urban (2.5 μ M GlpG in 50 mM Tris pH 7.4, 100 mM NaCl, 1 mM EDTA, 1 mM DTT and 0.1% (w/v) DDM).² Sample heating, aliquoting, absorbance and GlpG activity measurement were performed in the same way as in bicelles and liposomes.

In all measurements, absorbance at 320 nm and GlpG activity for the samples that had been incubated at each temperature were normalized relative to those at 25°C, respectively.

Cloning of GlpG Variants for *In Vivo* Degradation. *E. coli* AR3289 (W3110 *zad220::Tn10 sfhC21*) and *ftsH*-null AR3291 (W3110 *zad220::Tn10 sfhC21 Δ ftsH3::kan*) strains were generous gifts from Prof. Teru Ogura at Kumamoto University, Japan. They are derivatives of *E. coli* K-12 strain W3110 [F^- IN(*rrnD-rrnE*) I] from his laboratory.³ All *in vivo* constructs containing GlpG transmembrane (TM) domain (residues 87-276), N- or C-terminal degradation marker for FtsH (Dps_N, YccA_N, 108 or SsrA) and N-terminal FLAG or C-terminal HA epitope for Western blotting were cloned into pBAD/HisA vector using NcoI and XhoI restriction sites. Control plasmids were constructed with either FLAG epitope at the N-terminus or HA epitope at the C-terminus in the absence of the markers. In case of GlpG with HA epitope, it was susceptible to degradation by FtsH in the absence of specific markers (**Figure S3c**). Thus, we added two tandem Asp residues (DD) at the end of HA epitope (GlpG-HA-DD). This construct was not recognized by FtsH and used as a control.

GlpG Degradation Assay *In Vivo*. *E. coli* AR3289 (+*ftsH*) and AR3291 (*-ftsH*) strains were transformed with each GlpG variant plasmid. 7 mL of LB containing 100 μ g/mL of ampicillin was inoculated with a single colony and cells were grown for 18 h at 37°C for AR3289 and 30°C for AR3291. OD_{600 nm} was measured to check growth. When OD_{600 nm} reached in 1.5–1.7 (AR3289) and 0.8–1.0 (AR3291), GlpG expression was induced by addition of 0.2% (w/v) arabinose at 37°C for 1 h. Then protein synthesis was blocked by addition of 300 μ g/mL spectinomycin, immediately followed by collection of the sample at time 0. To monitor degradation over time, samples were further incubated at 37°C in a shaker at 180 rpm. 600 μ L of aliquot of each sample was taken at subsequent time points. All samples were frozen in liquid nitrogen immediately after collection. For immunodetection, thawed cells were spun down at 13,000 rpm for 3 min using a bench-top centrifuge (Eppendorf, 5424R). Depending on their absorbance, cell pellets were resuspended in TE Buffer (10 mM Tris-HCl, 1 mM EDTA, pH 8.0) and mixed with protein sample buffer (final concentration of 2% SDS (w/v), 0.1% (w/v) bromophenol blue, 10% glycerol (v/v), 1% (v/v) BME, 50 mM Tris-HCl, pH 6.8). The mixtures were sonicated for 10–30 sec prior to SDS-PAGE. 4–20% Mini-PROTEAN TGX gels (Bio-Rad) were used in all electrophoresis. To monitor GlpG degradation by FtsH, Western blotting analysis against HA or FLAG epitopes was performed. Epitope-tagged proteins were transferred to a PVDF membrane (Bio-Rad). The following procedures were performed according to the protocol provided by manufacturers. GlpG variants containing HA epitope were probed with HRP-conjugated anti-HA monoclonal antibody (Thermo Fisher Scientific, 1:1000 dilution). GlpG variants with FLAG epitope were detected using rabbit monoclonal anti-FLAG primary antibody (Cell Signaling Technology, 1:1000 dilution) and anti-rabbit IgG-HRP secondary

antibody (Cell Signaling Technology, 1:2000 dilution). Chemiluminescent detection was performed using Clarity Western ECL substrate (Bio-Rad) and ChemiDoc Imager (Bio-Rad).

Cloning and Mutagenesis of GlpG for *In Vitro* Degradation. Variants of GlpG TM domain (residues 87–276) fused to N-terminal maltose binding protein (MBP) followed by TEV cleavage site (TEV_{cleavage}) were cloned into pET30a vector using NdeI and XhoI restriction sites. The resulting expression plasmids encode the proteins with an N-terminal His₆-tag (His₆-MBP-TEV_{cleavage}-GlpG). Using this as a base construct, a degradation marker for FtsH was fused to the N-(Dps_N or YccA_N) or C-terminus (108 or SsrA) of GlpG. Cysteine mutant G172C was generated by QuikChange site-directed mutagenesis for thiol-reactive fluorophore labeling.

E. coli BL21(DE3) RP cells transformed with a GlpG plasmid were cultivated on selection plates (50 mg/L kanamycin) at 37°C. A liquid culture was inoculated with a single colony and cultured in LB media (50 mg/L kanamycin) overnight at 37°C, until reaching the stationary phase. The overnight culture was used to inoculate a fresh LB media (50 mg/L kanamycin) and the culture was grown at 37°C until an OD_{600nm} of 1.0, at which a final concentration of 0.5 mM IPTG was added. Culture was further grown 16 h at 15°C.

Purification of GlpG Variants for *In Vitro* Degradation Assay. His₆-MBP-TEV_{cleavage}-GlpG possessing a degradation marker was expressed in *E. coli* BL21(DE3) RP cells. Cells were harvested and resuspended in 1/50 culture volume of 50 mM Tris-HCl buffer solution (pH 8.0) containing 0.5 mM TCEP, 5 mM EDTA and 0.5 mM PMSF. The resuspended cells were lysed five times using pressure homogenizer. The lysate was centrifuged at 6,000 rpm for 30 min in F21 rotor using a Sorvall RC6+ centrifuge. The supernatant was centrifuged to obtain the total membrane fraction at 28,000 rpm for 2 h in Type 45 Ti rotor using ultracentrifuge (Beckman-Coulter). The membrane pellets were resuspended in 1/100 culture volume of 50 mM Tris-HCl buffer solution (pH 8.0) containing 200 mM NaCl and 0.5 mM TCEP using tissue homogenizer. The membrane resuspension was solubilized by addition of 1/100 culture volume of solubilization buffer (pH 8.0) containing 50 mM Tris-HCl, 2% (w/v) n-decyl-β-D-maltoside (DM, Anatrace), 200 mM NaCl, 0.5 mM TCEP, and 0.5 mM PMSF followed by ultracentrifugation at 12,000 rpm for 30 min in Type 45 Ti rotor. His₆-MBP-TEV_{cleavage}-GlpG in the supernatant was purified using Ni²⁺-NTA affinity chromatography (1 mL resin per liter culture). After removal of excess imidazole in a desalting column (Bio-Rad), the linker between His₆-MBP and GlpG was cleaved using TEV protease with an N-terminal His₇-tag (His₇-TEV protease) ([GlpG]/[TEV protease] = 5) after 6 h of gentle stirring at room temperature. 1 mL of Ni-NTA resin was added to the reaction mixture to bind His₇-TEV protease and His₆-MBP. GlpG portion was isolated in the flow-through and further concentrated using an Amicon centrifugal filter unit (Millipore Sigma, 10 kDa MWCO). The protein concentration was measured using absorbance at 280 nm ($\epsilon_{280nm} = 69,940 \text{ M}\cdot\text{cm}^{-1}$)

NBD-labeling of GlpG Variants. ~30 μM of purified single-cysteine mutant (G172C) of GlpG variants in 0.5% DM, 50 mM Tris-HCl and 200 mM NaCl (pH 8.0) was incubated with 10 times molar excess of TCEP for 1 h at room temperature. 15 times molar excess of thiol-reactive, environment-sensitive fluorophore IA-NBD amide dissolved in DMSO (~10 mg/mL) was added to the mixture while vortexing. Labeling reaction was incubated at 4°C overnight in the dark. Excess free labels were removed by dialysis against buffer containing 0.2% DM, 50 mM Tris-HCl, and 200 mM NaCl (pH 8.0) and a desalting column. Typically, the labeling efficiency of NBD ranged from 1.0–1.2 as determined by comparing the concentration of NBD measured by

UV-Vis absorbance ($\epsilon_{480\text{nm}} = 23,500 \text{ M}\cdot\text{cm}^{-1}$) to the concentration of GlpG measured by DC protein assay (Bio-Rad).

***In Vitro* GlpG Degradation Assay using NBD Fluorescence.** Degradation of NBD-labeled GlpG variants by FtsH was measured in 3% (w/v) bicelles (DMPC/DMPG/CHAPS, $q = 2.8$). To ensure integration of the model substrate GlpG into bilayers, GlpG was first reconstituted in DMPC/DMPG liposomes with the following protocol: Mixed dried lipid ([DMPC]:[DMPG] = 3:1) was dispersed in 20 mM HEPES (pH 7.6) 100 mM KCl, 15% glycerol, 0.1% BME and 4% β -OG to a final lipid concentration of 3% (w/v). The NBD-labeled GlpG stock solution (100–300 μM) in DM was mixed with the solubilized lipids to a final concentration of 50–100 μM and incubated on ice for 1 h. The mixture was dialyzed against $\times 350$ sample volumes of 20 mM HEPES (pH 7.5), 100 mM KCl, 15% glycerol, 0.1% BME buffer solution, with four buffer exchanges over 48 h at 4°C (10 kDa cutoff dialysis tubing, Thermo Fisher Scientific), followed by incubation with Bio-Beads (Bio-Rad, 0.2 mg/mL suspension) for 16 h at room temperature for further removal of residual detergents. The resulting proteoliposomes were extruded through a 0.2 μM pore size polycarbonate membrane (Sigma). The total phospholipid concentration was determined by an organic phosphate assay. Based on the measured total lipid concentration, desired amount of CHAPS was added to form bicelles with $q = 2.8$. The final concentration of NBD-labeled GlpG in bicelles was determined by DC assay.

Measurements of time-dependent degradation of GlpG were performed in 3% bicellar solution (20 mM HEPES, pH 7.5, 100 mM KCl, 15% glycerol, 0.1% BME, and 400 μM ZnCl_2) containing various concentrations of NBD-labeled GlpG and an ATP regeneration system (0.5 unit/100 μL pyruvate kinase and 10 mM phosphoenolpyruvic acid). FtsH was incorporated into bicelles by direct injection of FtsH stock solution in Triton X-100 (60-100 μM) to preformed bicelles at a final monomer concentration of 2 μM on ice. A total volume of 100 μL of each sample was transferred to a 96-well UV-compatible microplate (Greiner Bio-One) and sealed with a polyolefin film. Degradation of GlpG was initiated by addition of 2 mM ATP to each well and monitored by quenching of NBD fluorescence at 545 nm with an excitation wavelength of 485 nm on a SpectraMax M5 plate reader. The net change of NBD fluorescence induced by GlpG degradation was obtained by subtracting the time-dependent change of NBD fluorescence in the presence of ATP from that in the absence of ATP at each GlpG concentration. Data analysis and fitting equations are described in the following section.

Calculation of GlpG Degradation Rate. v_{deg} , GlpG degradation rate by each FtsH hexamer per minute, is defined as:

$$v_{\text{deg}} = \frac{\frac{\Delta F}{\min}}{\frac{\Delta F_{\infty}}{[\text{GlpG}]}} \times \frac{1}{[\text{FtsH}_6]} \quad (\text{Equation 4})$$

, where $\Delta F/\min$ and $\Delta F_{\infty}/[\text{GlpG}]$ were obtained from the slopes from **Figures S4i** and **S4j** (bottom), respectively.

Degradation rates of GlpG measured as a function of mole fraction of GlpG was fitted to the Michaelis-Menten equation:

$$v_{\text{deg}} = \frac{k_{\text{cat,deg}} X_{\text{GlpG}}}{K_{\text{m,deg}} + X_{\text{GlpG}}} \quad (\text{Equation 5})$$

, where v_{deg} is GlpG degradation rate by each FtsH hexamer per min, $k_{\text{cat,deg}}$ is maximal degradation turnover number of FtsH hexamer per min, and $K_{\text{m,deg}}$ is the mole fraction of GlpG (see below) at which the degradation rate reaches a half maximum. X_{GlpG} designates a mole fraction of GlpG out of total bicellar constituents ($X_{\text{GlpG}} = [\text{GlpG}]/([\text{DMPC}]+[\text{DMPG}]+[\text{CHAPS}]+[\text{GlpG}]+[\text{FtsH}])$).

The degradation rates were also fitted to the Hill equation:

$$v_{\text{deg}} = \frac{X_{\text{GlpG}}^{n_{\text{H,deg}}}}{K_{\text{m,deg}}^{n_{\text{H,deg}}} + X_{\text{GlpG}}^{n_{\text{H,deg}}}} \quad (\text{Equation 6})$$

, where $n_{\text{H,deg}}$ is Hill constant of GlpG degradation by FtsH hexamer.

GlpG Unfolding Kinetics Measured by Steric Trapping in Bicelles. Steric trapping for measuring the spontaneous unfolding rate (k_{U}) of GlpG was achieved by shifting the reaction flux towards the unfolding direction using wild type monovalent streptavidin (mSA-WT) possessing high-affinity to biotin (mSA-WT; $K_{\text{d,biotin}} \approx 10^{-14}$ M; $k_{\text{on,biotin}} \approx 10^7$ M⁻¹ s⁻¹; $k_{\text{off,biotin}} \approx$ weeks).⁴⁻⁶ For steric trapping of GlpG in bicelles, His₆-MBP-TEV_{cleavage}-GlpG possessing the 108 degradation tag was modified to contain two cysteine residues by site-directed mutagenesis at Pro95/Gly172 or Gly172/Val267. These GlpG variants were purified as described above and doubly-labeled with thiol-reactive BtnPyr-iodoacetamide.¹ Resulting double-biotin GlpG variants in DDM was mixed with bicelle stocks (DMPC/DMPG/CHAPS, $q = 2.8$) to a final condition of 2.5 μM GlpG, 3% (w/v) bicelles, 20 mM HEPES (pH 7.5), 100 mM KCl and 0.05% (v/v) sodium azide. GlpG in bicelles was allowed to equilibrate on ice for 1 h and at room temperature for 30 min before use.

Unfolding kinetics of GlpG was measured using its site-specific proteolytic activity as an unfolding readout. Stock solution of SN-LacYTM2 (**Figure S2a**), the model substrate of GlpG, in bicelles was prepared by mixing SN-LacYTM2 in DDM with bicelles to a final condition of 50 μM SN-LacYTM2, 3% (w/v) bicelles, 20 mM HEPES (pH 7.5), 100 mM KCl and 0.05% (v/v) sodium azide. SN-LacYTM2 in bicelles was allowed to equilibrate on ice for 1 h and at room temperature for 30 min before use.

To initiate the unfolding reaction, wild type monovalent streptavidin (mSA-WT Y83C variant¹) labeled with non-fluorescent quencher DABMI (Setareh Biotech) was added to the GlpG-bicelle complex for steric trapping. The unfolding reaction was incubated at 37°C up to 10 days. The GlpG samples without mSA were used as a control. At desired time points, the reaction mixtures at 37°C were taken and equilibrated to room temperature for 15 min before GlpG activity assay.

The activity assay was performed by mixing 5 μL GlpG in bicelle without or with mSA with 5 μL of SN-LacYTM2 in bicelle and 15 μL of buffer solution (20 mM HEPES, 100 mM KCl, pH 7.5), and incubated at room temperature for 25 min. The time dependent increase of the unfolded fraction, which is represented by the decrease of the site-specific cleavage product of SN-LacYTM2 (SN-ΔLacYTM2) was measured by SDS-PAGE. 25 μL of 6% SDS sample loading

buffer was added to terminate the cleavage reaction of SN-LacYTM2 by GlpG and then the mixture was loaded on 12.5% TGX gels (Bio-Rad).

The unfolded fraction of GlpG at each time point was quantified in the following way: First, the band intensity of the cleavage product SN- Δ LacYTM2 representing the activity of GlpG was obtained using ImageJ software (<https://imagej.nih.gov/ij/index.html>) for the samples containing GlpG as control and the samples containing GlpG and mSA as experiment. We had difficulties in resolving the reactant (SN-LacYTM2) band and the product band (SN- Δ LacYTM2) from the digitized intensity profile. In that case, we applied double Gaussian function to obtain the intensity of the product band in the Origin program (OriginLab). The unfolded fraction was defined as the relative activity, which was calculated as the ratio of the band intensity with mSA to that without mSA. To obtain the spontaneous unfolding rate k_U , the relative activities were plotted as a function of time and fit to an equation for first-order reaction kinetics:

$$y = y_0 + Ae^{-k_U t} \quad (\text{Equation 7})$$

, where y is relative activity; y_0 is the minimal activity left after unfolding; A is the amplitude change during the unfolding reaction; k_U is the spontaneous unfolding rate constant; t is time.

GlpG Unfolding Kinetics Measured by Steric Trapping in DDM. To initiate the unfolding reaction by steric trapping in DDM, 20 times molar excess mSA-WT (Y83C) labeled with DABMI was added to each double-biotin GlpG variant, 95/172_N-BtnPyr₂ or 172/267_C-BtnPyr₂ at 1 μ M. The unfolding reaction was incubated at a desired temperature (from 9°C to 37°C) for up to a week. As controls, GlpG samples without mSA were incubated in parallel at the same temperature used for the samples with mSA. Activity assay was carried out using the fluorescence-based GlpG activity assay developed in the Hong lab.¹ Briefly, at each desired time point, 45 μ L of GlpG sample was taken out from the unfolding reaction and the activity assay was initiated by addition of 10 times molar excess of the NBD-labeled SN-LacYTM2 substrate to GlpG in DDM. Time-dependent changes of NBD fluorescence were monitored in 96-well plate using SpectraMax M5e plate reader (Molecular Devices) with excitation and emission wavelengths of 485 nm and 535 nm, respectively. The fluorescence change for each sample containing GlpG and the substrate was normalized to the fluorescence change of the sample containing the substrate alone. GlpG activity was represented by the fitted slope of a linear region of the fluorescence change as a function of time. The unfolded fraction at each time point was obtained by taking the ratio of the activity with mSA to that without mSA. The time-dependent unfolded fraction was fitted against time using equation 7 to obtain the spontaneous unfolding rates k_U in DDM.

Computing Dislocation Free Energy of GlpG. Free energy of dislocation ($\Delta G_{\text{dislocation}}$) was defined as the free energy required to transfer the whole TM helices of fully unraveled GlpG from the lipid bilayer to water. It can be approximated by summing up the free energy changes in Stage 2-1 (backbone unfolding of TM helices in the bilayer) and Stage 2-2 (transfer of the unfolded polypeptide from bilayer to water) (**Figure S8**) as follows:

$$\Delta G_{\text{dislocation}} = \sum_{\text{H-bonds}} \Delta G_{\text{H-bond, backbone}} + \sum_{\text{residues}} T\Delta S_{\text{side-chain}} + \sum_{\text{residues}} \Delta G_{\text{transfer, residueX}} \quad (\text{Equation 8})$$

, where $\Delta G_{\text{H-bond,backbone}}$ is the free energy change for breaking a backbone hydrogen bond in the TM α -helices inside the lipid bilayer,⁷ $T\Delta S_{\text{side-chain}}$ is the change in side-chain entropy for helix unfolding,⁸ and $\Delta G_{\text{transfer, residueX}}$ is the free energy change for transferring the whole residue X from the bilayer to water. Here $\Delta G_{\text{transfer, residueX}}$ can be computed as

$$\Delta G_{\text{transfer, residueX}} = \Delta G_{\text{transfer, Ala}} + \Delta G_{\text{transfer, Ala} \rightarrow \text{residueX}} \quad (\text{Equation 9})$$

, where $\Delta G_{\text{transfer, Ala}}$ is the transfer free energy of whole residue Ala,⁹ and $\Delta G_{\text{transfer, Ala} \rightarrow \text{residueX}}$ is the side-chain transfer free energy of residue X with respect to Ala. Here it was assumed that the depth-dependence of $\Delta G_{\text{H-bond,backbone}}$ and $\Delta G_{\text{transfer, Ala, whole residue}}$ was not significant.¹⁰

The side-chain transfer free energy $\Delta G_{\text{transfer, Ala} \rightarrow \text{residueX}}$ was determined using the depth-dependent general transfer free energy profile (GeTFEP),¹¹ which is obtained by computing the side-chain transfer free energies in β -barrel membrane proteins.^{12,13} GlpG structure of PDB ID 2XOW was used, with the TM segments determined using the Orientations of Proteins in Membranes (OPM) database.¹⁴ The C_{α} coordinates of each TM residue and the thickness of TM segments were used to determine the relative depth d of that residue, which is then used for calculating the side-chain transfer free energy $\Delta G_{\text{transfer, Ala} \rightarrow \text{residueX}}(d)$ using GeTFEP.

$$\Delta G_{\text{transfer, Ala} \rightarrow \text{residueX}}(d) = \sum_{i=0}^3 p_{X,i} \cdot d^i \quad (\text{Equation 10})$$

, where $p_{X,i}$ is the i -th coefficients of residue X in GeTFEP. The sequence of GlpG structure with a bound inhibitor (PDB ID 2XOW) is identical to that of the apo-structure (PDB ID) 3B45. The root-mean-square deviation (RMSD) between these two structures is 0.60Å.

QUANTIFICATION AND STATISTICAL ANALYSIS

Throughout the manuscript, the data are represented as the average \pm SEM or \pm STD of fit. All experiments were performed at least in triplicates unless specified. The exact value of n for every dataset of this paper is provided:

Further information regarding statistical analysis can be found in the figure legends.

Quantitative band analysis of the resulting SDS-PAGE gel and Western blot was carried out using ImageJ (<https://imagej.nih.gov/ij/index.html>) software to determine the band intensity, the fraction of substrate cleaved at each timepoint.

SUPPORTING TABLES

Table S1. Kinetic parameters of ATPase activity of FtsH in various lipid environments

	Michaelis-Menten		Hill coefficient
	$k_{\text{cat,ATP}}^{\text{a}}$ ($\text{min}^{-1} \text{FtsH}_6^{-1}$)	$K_{\text{m,ATP}}^{\text{a}}$ (μM)	$n_{\text{H,ATP}}^{\text{b}}$
DMPC/CHAPS	170 ± 4	310 ± 30	0.9 ± 0.1
DMPC/DMPG/CHAPS	128 ± 4	220 ± 30	1.0 ± 0.1
Triton X-100	51 ± 2	400 ± 50	1.0 ± 0.1
<i>E. coli</i> lipids	118 ± 3	700 ± 70	0.9 ± 0.1
DMPC/DMPG	64 ± 2	330 ± 50	0.9 ± 0.1
CHAPS	21 ± 2	4,700 ± 1,000	0.8 ± 0.2

All measurements were performed with $[\text{FtsH}] = 2 \mu\text{M}$ in 3% (w/v) total amphiphile concentration at 37 °C.

^a $k_{\text{cat,ATP}}$ and $K_{\text{m,ATP}}$ values are from nonlinear least square fits of data in **Figure 1b** to the Michaelis-Menten equation (See **Supporting Methods** Equation 2).

^b $n_{\text{H,ATP}}$ was obtained from nonlinear least squares fits of data in **Figure 1b** to the Hill equation (See **Supporting Methods** Equation 3).

Table S2. Folding parameters of water-soluble model substrates and GlpG for AAA+ proteases

	ΔG_{U} (kcal/mol)	k_{U} (min^{-1})	T_{m} (°C)
DHFR	6.1 ^a	5×10^{-2} ^b	54 ^c
GFP	N/A ^d	~years ^e	76 ^f
barnase	8.8 ^g	$\sim 10^{-4}$ ^h	70 ⁱ
Arc	10.9 ^j	6 ^k	59 ^l
PhoA	N/A	N/A	~70 ^m
DGK	16 ⁿ	$< \sim 10^{-5}$ ^o	~80 ^p
GlpG	~4 ^q , 4.7 ^r , 5.8 ^s	3.4×10^{-3} ^q $2 - 3 \times 10^{-4}$ ^t	>85 ^u , 71 ^v

ΔG_{U} : thermodynamic stability

k_{U} : spontaneous unfolding rate

T_{m} : thermal melting temperature

^a measured at room temperature¹⁵

^b measured at 15°C¹⁶

^c from reference¹⁷

^d No available data

^e from reference¹⁸

^f from reference¹⁹

^g measured at room temperature²⁰

^h measured at room temperature²¹

Continued

ⁱ from reference²²

^j measured at room temperature²³

^k measured at room temperature²⁴

^l from reference²⁵

^m from reference²⁶

ⁿ measured in SDS/decylmaltoside mixed micelles²⁷

^o measured in *n*-octylglucoside by steric trapping⁵

^p measured in dodecylmaltoside²⁸

^q measured by single-molecule force spectroscopy in neutral DMPC/CHAPSO bicelles at room temperature²⁹

^r C-subdomain, measured by steric trapping at room temperature¹

^s N-subdomain, measured by steric trapping at room temperature¹

^t measured in DMPC/DMPG/CHAPS bicelles at 37°C in this study

^u measured in DMPC/DMPG/CHAPS bicelles and *E. coli* lipids in this study

^v measured in dodecylmaltoside²

Table S3. Kinetic parameters of GlpG degradation by FtsH

	Michaelis-Menten		Hill coefficient
	$k_{\text{cat,deg}}^{\text{a}}$ ($\text{min}^{-1} \text{FtsH}_6^{-1}$)	$K_{\text{m,deg}}^{\text{a}}$ (X_{GlpG})	$n_{\text{H,deg}}^{\text{b}}$
GlpG-108	$2.7 \pm 0.1 \times 10^{-1}$	$3.7 \pm 0.5 \times 10^{-5}$	0.6 ± 0.1
GlpG-SsrA	$2.5 \pm 0.1 \times 10^{-1}$	$3.0 \pm 0.4 \times 10^{-5}$	0.7 ± 0.1
YccA _N -GlpG	$1.6 \pm 0.1 \times 10^{-1}$	$6.3 \pm 0.7 \times 10^{-5}$	0.8 ± 0.1
Dps _N -GlpG	$1.6 \pm 0.1 \times 10^{-1}$	$9.0 \pm 0.8 \times 10^{-5}$	1.1 ± 0.1
GlpG _{M100A} -108	$3.7 \pm 0.1 \times 10^{-1}$	$2.8 \pm 0.6 \times 10^{-5}$	0.5 ± 0.1
YccA _N -GlpG _{M100A}	$2.6 \pm 0.1 \times 10^{-1}$	$17.3 \pm 2.4 \times 10^{-5}$	0.9 ± 0.1
GlpG _{LLWF} -108	$2.2 \pm 0.1 \times 10^{-1}$	$2.3 \pm 0.3 \times 10^{-5}$	1.2 ± 0.2

All measurements were performed with $[\text{FtsH}] = 2 \mu\text{M}$ in 3% (w/v) DMPC/DMPG/CHAPS bicelles at 37 °C.

^a $k_{\text{cat,deg}}$ and $K_{\text{m,deg}}$ values are from nonlinear least square fits of data in **Figures 3d, 5d and 5f** to the Michaelis-Menten equation (See **Supporting Methods** Equation 5).

^b $n_{\text{H,deg}}$ was obtained from nonlinear least squares fits of data in **Figures 3d, 5d and 5f** to the Hill equation (See **Supporting Methods** Equation 6).

Table S4. $\Delta G_{\text{dislocation}}$ of individual TM helices of GlpG using membrane-depth dependent transfer free energy

Helix ID	Helix Segment	Stage 2-1		Stage 2-2	Total
		$\Delta G_{\text{H-bond,backbone}}^{\text{a}}$	$T\Delta S_{\text{side chain}}^{\text{b}}$	$\Delta G_{\text{transfer,side chain, Ala}\rightarrow\text{residue}X^{\text{c}}} + \Delta G_{\text{transfer,Ala, whole residue}}^{\text{d}}$	
TM1	95-113	79.50	-23.75	14.46	70.21
TM2	148-166	79.50	-23.75	14.36	70.11
TM3	171-190	84.80	-25.00	9.60	69.40
TM4	201-214	53.00	-17.50	7.15	42.65
TM5	227-241	58.30	-18.75	12.70	52.25
TM6	252-267	68.90	-21.25	8.83	56.48
All TM helices		424.00	-130.00	67.10	361.11

^a $\Delta G_{\text{H-bond,backbone}}$ = Number of H bond per TM helix \times 5.3 kcal/mol = (Number of TM residues – 4) \times 5.3 kcal/mol.⁷ This value falls into the range of stronger backbone hydrogen bonds ($\Delta G^{\text{HB}} = 4\text{--}8$ kcal/mol) experimentally determined in detergent micelles.³⁰

^b $T\Delta S_{\text{side chain}}$: Because one peptide bond is shared by two residues, one residue contributes -1.25 kcal/mol of $T\Delta S_{\text{side chain}}$ ⁸

^c $\Delta G_{\text{transfer,side chain, Ala}\rightarrow\text{residue}X}$: computationally derived depth-dependent hydrophobicity scale relative to Ala residue¹¹

^d $\Delta G_{\text{transfer,Ala, whole residue}} = 0.16$ kcal/mol, knowledge-based unified hydrophobicity scale for the whole Ala residue⁹

Table S5. The effects of bound substrates on ATPase activity of FtsH

	Michaelis-Menten		Hill coefficient
	$k_{\text{cat,ATP}}^{\text{a}}$ ($\text{min}^{-1} \text{FtsH}_6^{-1}$)	$K_{\text{m,ATP}}^{\text{a}}$ (X_{GlpG})	$n_{\text{H,ATP}}^{\text{b}}$
No substrate	109 \pm 2	0.17 \pm 0.02	1.0 \pm 0.1
+ GlpG-108	99 \pm 3	0.20 \pm 0.03	0.7 \pm 0.1
+ YccA _N -GlpG	82 \pm 3	0.17 \pm 0.02	0.8 \pm 0.1

All measurements were performed with [FtsH] = 2 μM in 3% (w/v) DMPC/DMPG/CHAPS bicells at 37 $^{\circ}\text{C}$.

^a $k_{\text{cat,ATP}}$ and $K_{\text{m,ATP}}$ values are from nonlinear least square fits of data in **Figure S9** to the Michaelis-Menten equation (See **Supporting Methods** Equation 2).

^b $n_{\text{H,ATP}}$ was obtained from nonlinear least squares fits of data in **Figure S9** to the Hill equation (See **Supporting Methods** Equation 3).

Table S6. Comparison of ATP costs during degradation of several model proteins by AAA+ proteases

AAA+ protease	Substrate	Substrate type	Number of ATP hydrolysis min ⁻¹ substrate ⁻¹	Number of residues	Number of ATP hydrolysis/residue
FtsH ^a	GlpG-108	membrane	380 – 550	228	1.7–2.5
FtsH ^b	σ^{32}	water-soluble	140	289	0.5
ClpXP ^c	Titin-I27-SsrA	water-soluble	644	98	6.6
ClpXP ^d	GFP-SsrA	water-soluble	146	268	0.5
Lon ^e	β -galactosidase (3-93)	water-soluble	175	91	1.9
Lon ^f	cp6-sul20 ^g / cp7-sul20 ^g	water-soluble	60/ 186	284	0.2/ 0.7
PAN ^h	casein	water-soluble	312	220	1.4

^a from this work

^b from reference³¹

^c from reference³²

^d from reference³³

^e from reference³⁴

^f from reference³⁵

^g circular-permuted superfolder GFP variants

^h from reference³⁶

SUPPORTING FIGURES

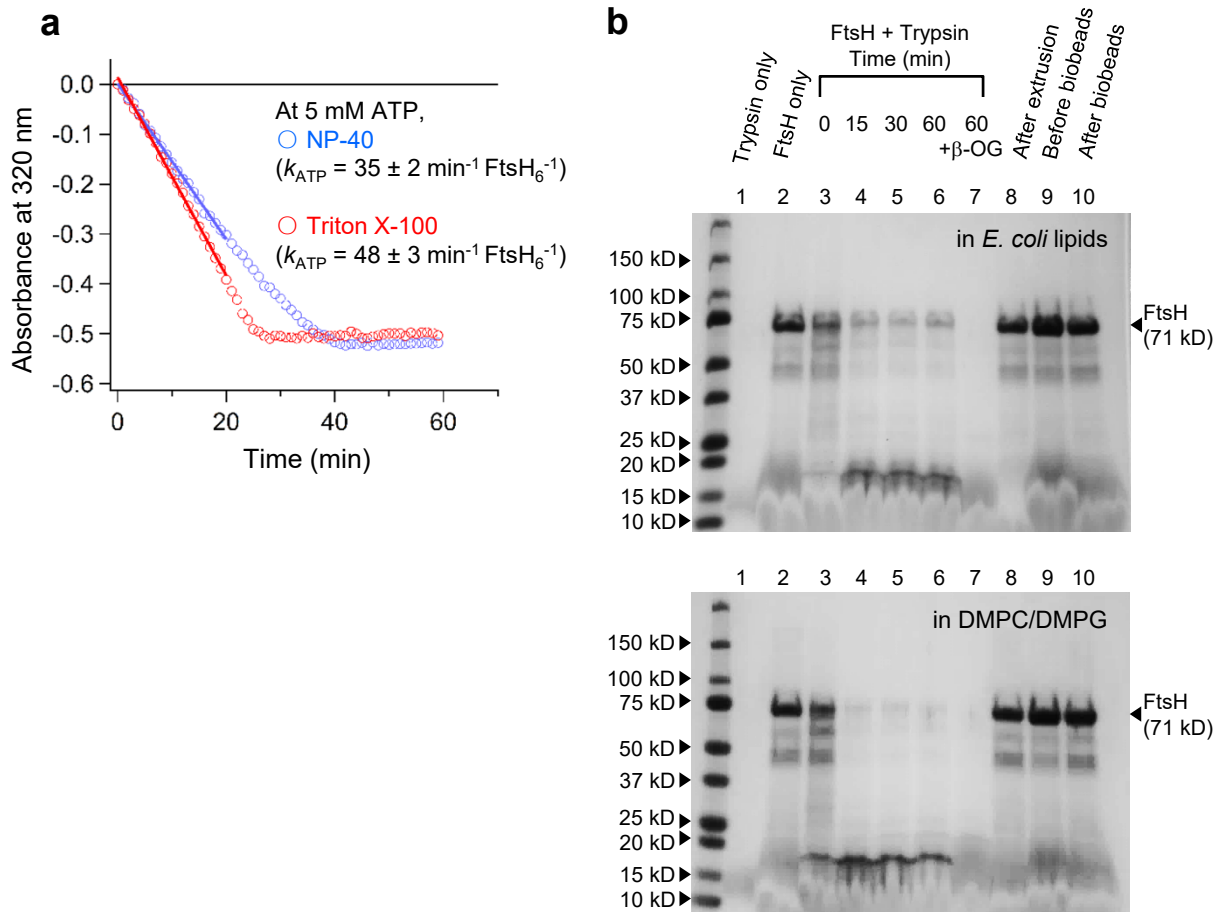


Figure S1, Related to Figure 1. ATPase activity of FtsH as model degradation machinery.

(a) Comparison of ATPase activity in detergent NP-40 and Triton X-100. Although both NP-40 and Triton X-100 had been widely used detergents in FtsH studies, we found that Triton X-100 supported ATP hydrolysis slightly better. See **Supporting Methods** for detailed solution condition. ATP hydrolysis was measured by an enzyme-coupled assay in the presence of 5 mM ATP at 37°C.

(b) Analysis of the orientation distribution of FtsH in liposomes and tracking the protein loss during the reconstitution (see **Figure 1b**). FtsH purified in Triton X-100 (lanes 2) was reconstituted in (*top*) *E. coli* phospholipids or (*bottom*) DMPC/DMPG lipids for ATPase assay. For reconstitution, extruded liposomes (58 mM) were soaked with 0.5 mM ($2 \times \text{CMC}$) Triton X-100, and detergent-solubilized FtsH was added to the lipid-detergent mixture ($[\text{FtsH}] = 10 \mu\text{M}$, lanes 9). Detergents were gradually removed using biobeads at 25°C for 4 hr. The resulting proteoliposomes (lanes 10) were extruded again to remove protein aggregation. After these steps, ~60% of FtsH was lost (compare lanes 8 and 10). The orientation distribution of FtsH was analyzed by limited trypsin digestion (FtsH-to-trypsin mass ratio = 50), which proteolyzed its large cytoplasmic portion containing AAA⁺ and Zn²⁺ protease domains (52 kD; lanes 3-6). Solubilization of proteoliposomes with β -octylglucoside (β -OG) led to complete digestion of FtsH (lanes 7). Overall, >90% of FtsH was inserted into liposomes with its cytoplasmic portion pointing outside.

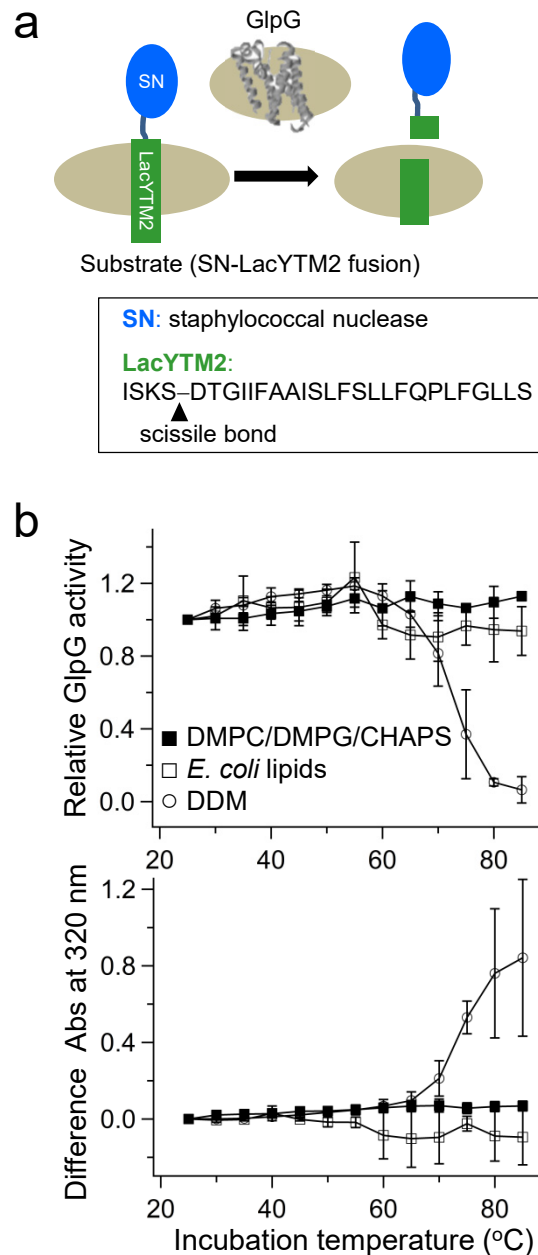


Figure S2, Thermostability of GlpG in various lipid environments.

(a) Activity assay of the model membrane substrate GlpG. Measuring proteolytic activity of GlpG using the second transmembrane (TM) domain of lactose permease of *E. coli* fused to staphylococcal nuclease (SN-LacYTM2: 25.7 kD) as a model substrate. GlpG cleaves the scissile peptide bond near the water-membrane interface of LacYTM2. This cleavage reaction can be measured by SDS-PAGE or fluorescence-based assay developed by the Hong group¹.

(b) Thermostability of GlpG measured by thermal (*top*) inactivation and (*bottom*) aggregation in DDM micelles, DMPC/DMPG/CHAPS bicelles and liposomes composed of *E. coli* phospholipids. The activity and absorbance measured at various temperatures were normalized to those at 25°C. Data are represented as mean \pm SEM ($n = 3$).

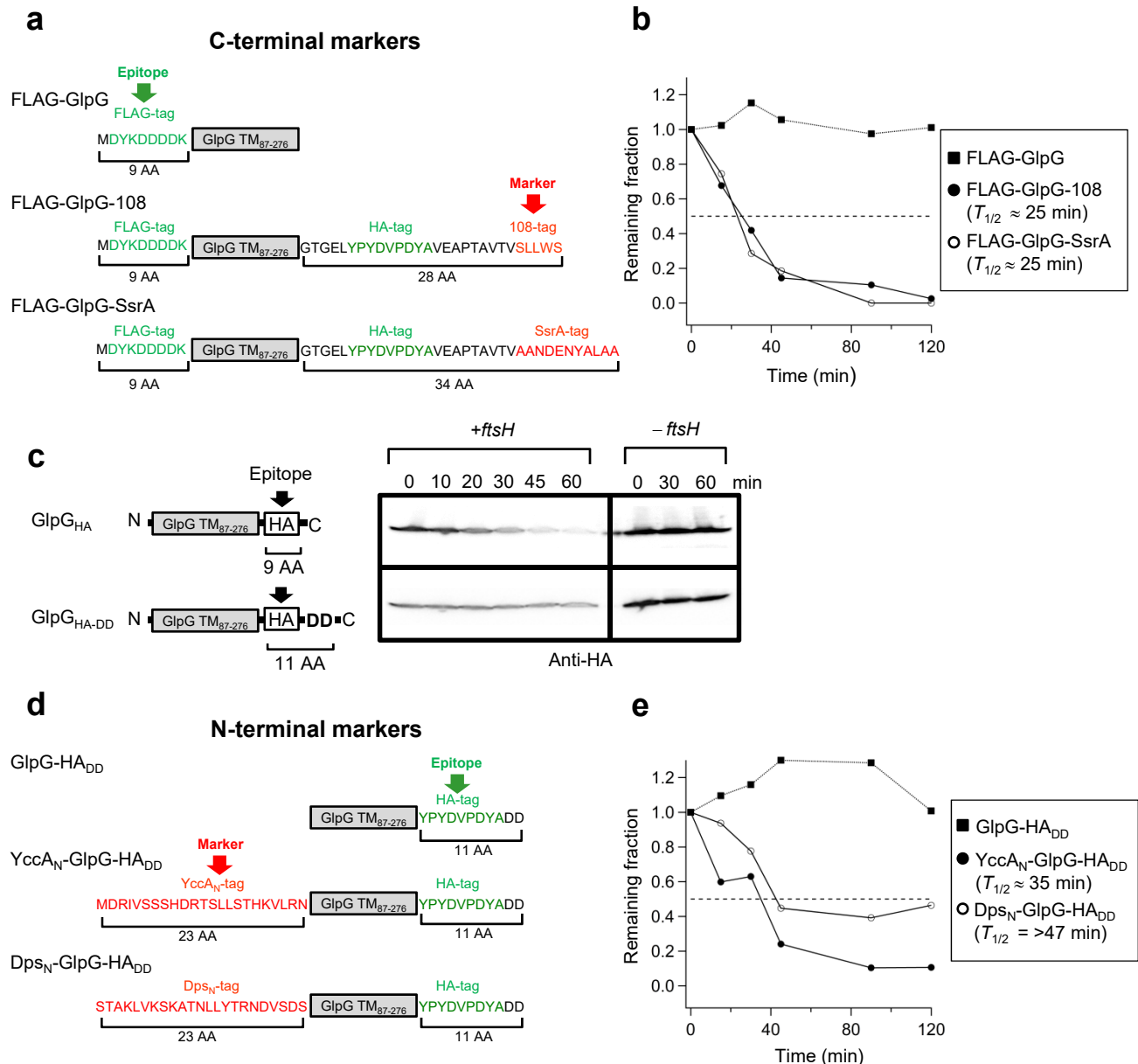


Figure S3, Related to Figure 2. Time-dependent degradation of GlpG variants *in vivo*.

(a) The constructs for measuring time-dependent degradation of GlpG possessing the C-terminal degradation markers, the 108-tag and the SsrA-tag.

(b) Quantification of time-dependent degradation of GlpG variants with the C-terminal markers in the *+ftsH E. coli* strain monitored by SDS-PAGE and Western blotting (see also **Figure 2b**).

(c) (Top) To investigate the effect of the N-terminal markers on GlpG degradation, the HA epitope was fused to the C-terminus of GlpG. However, the HA epitope induced unwanted degradation by FtsH even in the absence of a specific marker. (Bottom) Addition of two Asp residues (DD) to the C-terminus suppressed the unwanted degradation. Thus, using this as a control, the specific effect of the N-terminal markers (**Figure 2c** and **Figures S3d–e**) was studied.

(d) The constructs for measuring time-dependent degradation of GlpG possessing the N-terminal degradation markers, the YccA_N-tag and the Dps_N-tag.

(e) Quantification of time-dependent degradation of GlpG variants with the N-terminal markers in the *+ftsH E. coli* strain monitored by SDS-PAGE and Western blotting (see also **Figure 2c**).

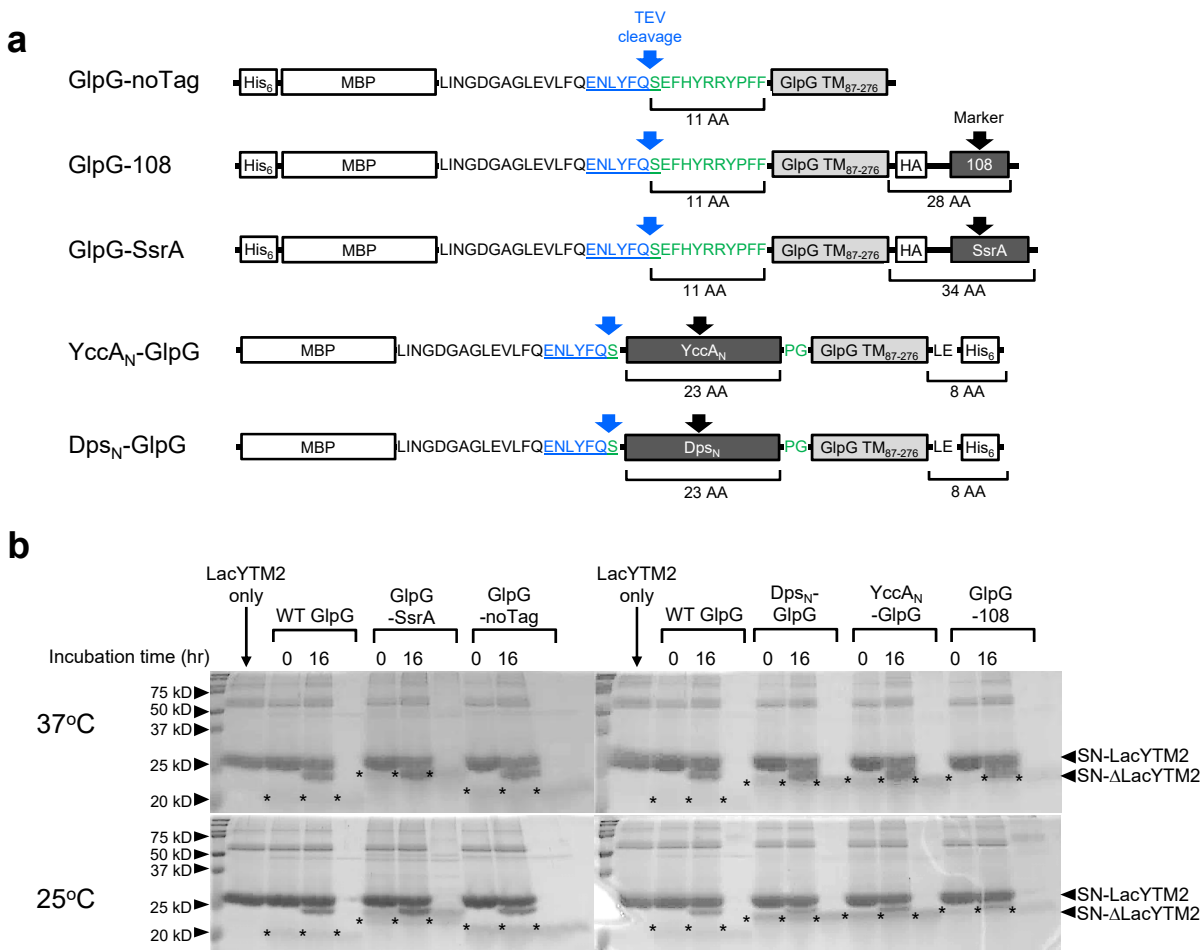
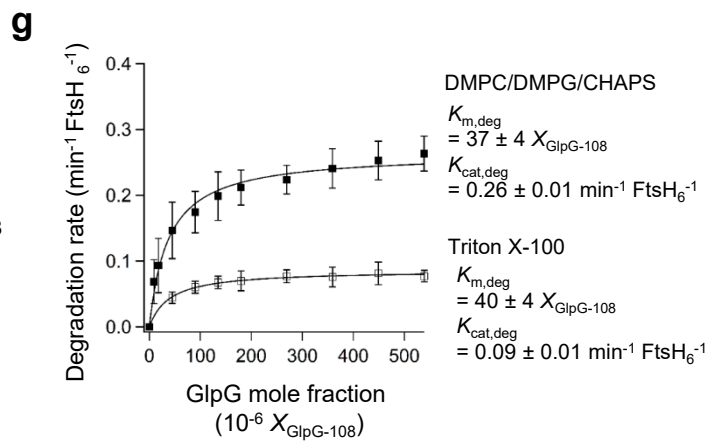
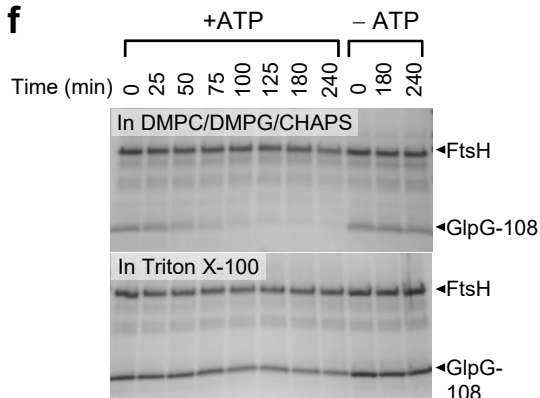
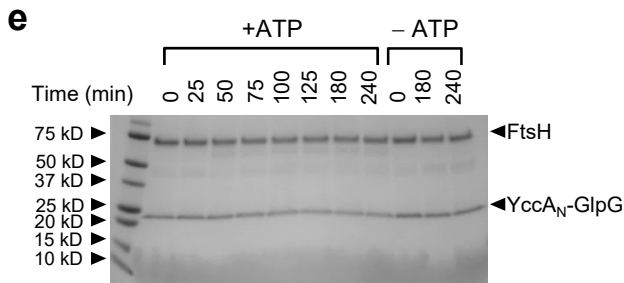
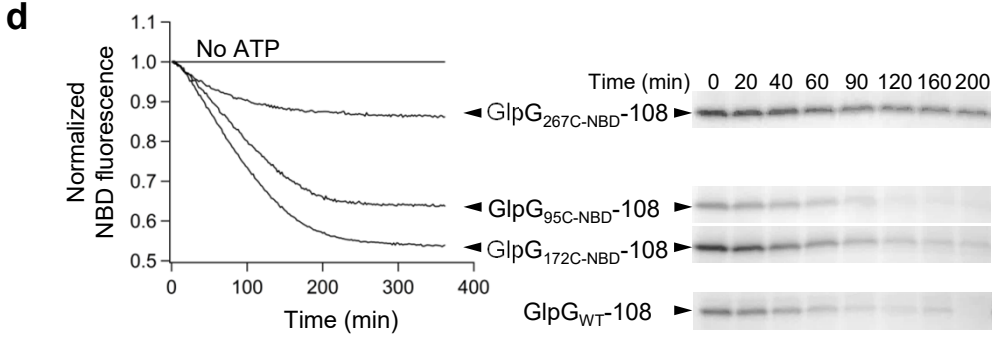
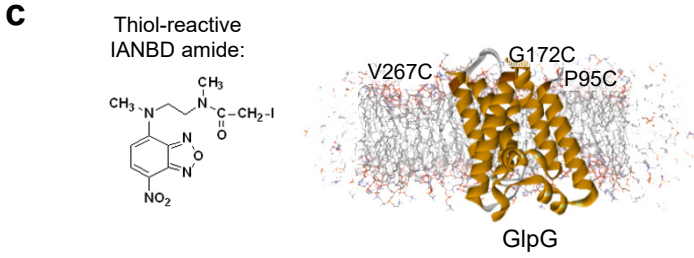


Figure S4, Related to Figure 3. FtsH-mediated degradation of GlpG in bicelles.

(a) The constructs for measuring time-dependent degradation of GlpG *in vitro*. These GlpG variants were expressed as maltose binding protein (MBP) fusions. GlpG possessing various degradation markers were isolated using TEV protease which cleaved the recognition sequence located in the linker between MBP and GlpG (see also **Supporting Methods** for more detailed cloning and purification information).

(b) Activity of GlpG variants with various degradation markers measured by SDS-PAGE (see also **Figure S2a**). This data show that all tested GlpG variants are fully functional and in the native conformation. The activity was measured under the same solution condition used for the degradation assay in 3% DMPC/DMPG/CHAPS bicelles (See **Supporting Methods** for detailed condition). Briefly, GlpG (2 μ M) and SN-LacYTM2 (10 μ M), which were separately reconstituted in bicelles, were mixed and incubated for 16 hr at each temperature. This reaction yielded the cleavage product SN- Δ LacYTM2. The asterisk marks (*) on the gel indicate the location of GlpG variants.



(Continued) Figure S4, Related to Figure 3. FtsH-mediated degradation of GlpG in bicelles.

(c) Optimization of the position for NBD labeling on GlpG to develop a fluorescence-based degradation assay. Three positions tested for single cysteine mutation (P95C, G172C and V267C) are located at the membrane-water interface on TM1, TM3 and TM6 helices to achieve both efficient labeling and partition of NBD to the nonpolar lipid environment.

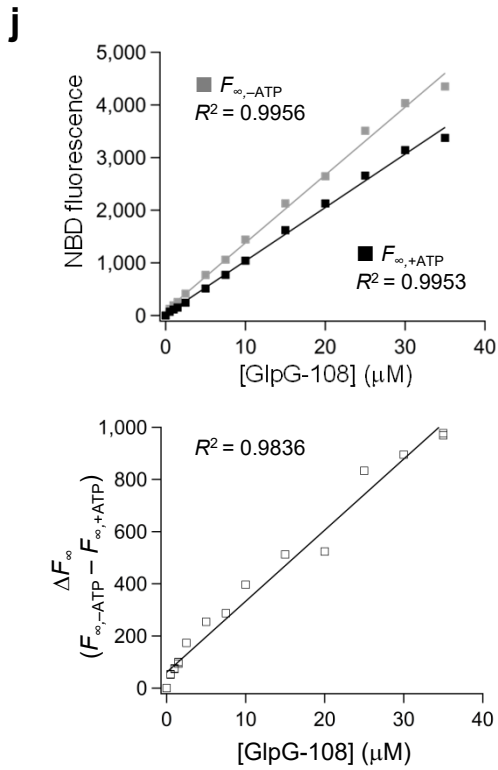
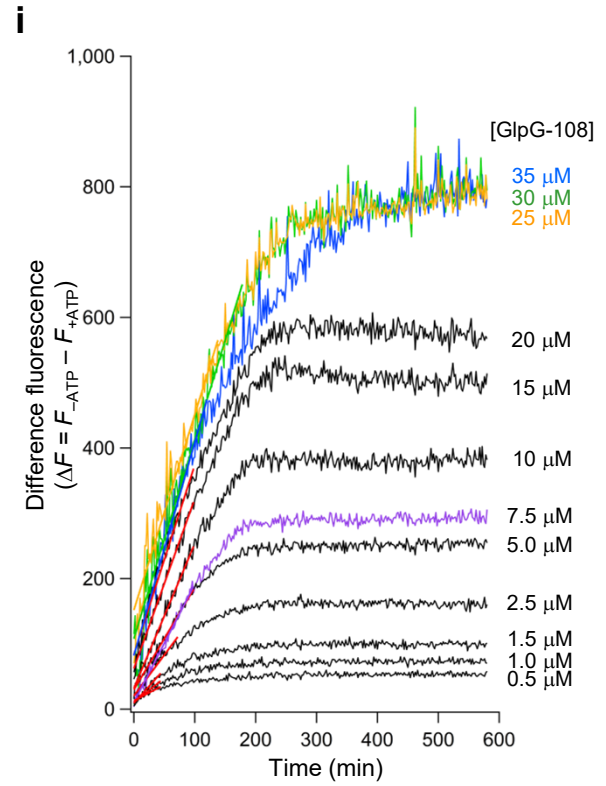
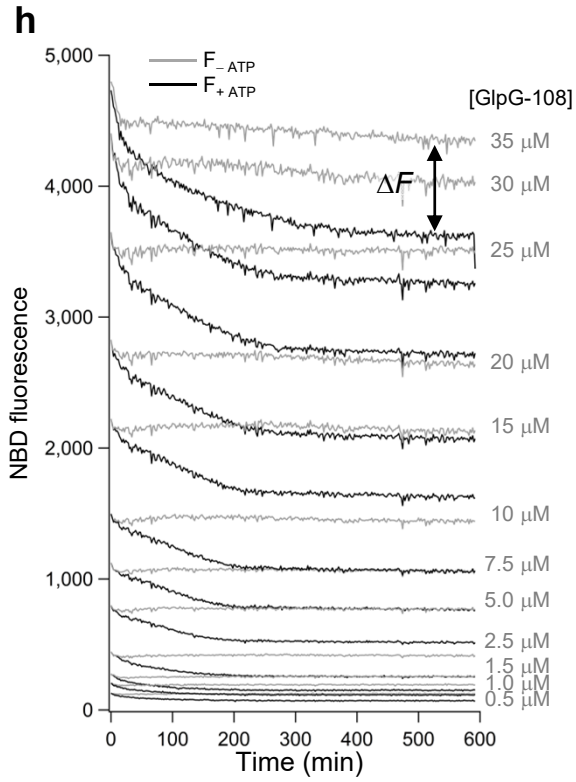
(d) The influence of the position of NBD-label on degradation rate and on the sensitivity of fluorescence signal. Time-dependent degradation of single-NBD labeled GlpG variants with the C-terminal 108 tag were measured using (*left*) NBD-fluorescence and (*right*) SDS-PAGE. GlpG_{172C-NBD}-108 was chosen because it exhibited the largest fluorescence change upon degradation among these variants and was degraded at a similar rate to wild-type GlpG-108 lacking Cys mutation (GlpG_{WT}-108) as seen from SDS-PAGE.

(e) The whole-gel image of SDS-PAGE monitoring time-dependent degradation of GlpG variant in bicelles (See also **Figure 3b**). This data shows that the site-specific protease GlpG did not significantly cleave FtsH over prolonged incubation.

(f–g) Comparison of GlpG degradation kinetics in bicelles and micelles.

(f) Comparison of time-dependent degradation of GlpG-108 (5 μ M) by FtsH (3 μ M) in 3% DMPC/DMPG/CHAPS bicelles and 3% Triton X-100 micelles monitored by SDS-PAGE.

(g) Michaelis-Menten plot of GlpG degradation measured at an increasing concentration of GlpG-108 (0.5–30 μ M) and a fixed concentration of FtsH (2 μ M) in 3% DMPC/DMPG/CHAPS bicelles and 3% Triton X-100. The reactions were performed in the presence of 5 mM ATP at 37°C. Data are represented as mean \pm SEM ($n = 3$). The detailed procedures to obtain degradation rates are described in **Figures S4h–l**.

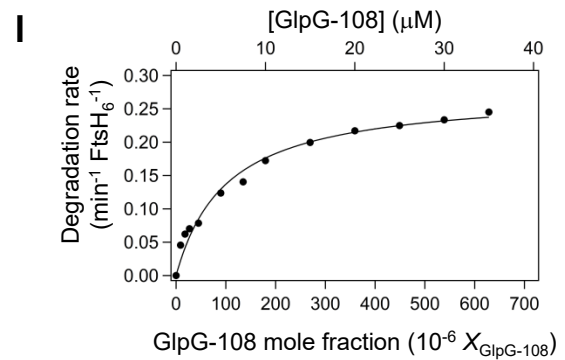


k

Initial GlpG egradation rate ($\text{min}^{-1} \text{FtsH}_6^{-1}$)

$$= \frac{\Delta F \text{ per min (from Figure S4i)}}{\Delta F_{\infty} \text{ per [GlpG-108] degraded (from Figure S4j)}} \times \frac{1}{[\text{FtsH}_6]}$$

$$= \frac{\frac{\Delta F}{\text{min}}}{\frac{\Delta F_{\infty}}{[\text{GlpG-108}]}} \times \frac{1}{[\text{FtsH}_6]}$$



(Continued) Figure S4, Related to Figure 3. FtsH-mediated degradation of GlpG in bicelles.

(h–l) Procedures to determine degradation rates of NBD-labeled GlpG using fluorescence. This is an example for GlpG-108_{G172C-NBD}. The assay was performed at a fixed concentration of FtsH (2 μ M) and increasing concentrations of GlpG-108 in buffer solution containing 3% (w/v) DMPC/DMPG/CHAPS bicelles at 37°C in the presence of a ATP regeneration system (See **Supporting Methods** for detailed solution condition).

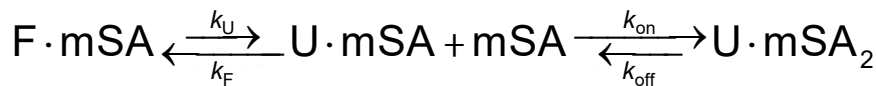
(h) Time-dependent NBD fluorescence was measured at various concentrations of GlpG-108 in the absence (F_{-ATP}) and presence (F_{+ATP}) of ATP.

(i) Time-dependent change of the net fluorescence intensity indicates GlpG degradation. It was obtained by subtracting the fluorescence intensity without ATP from that with ATP at each GlpG concentration ($\Delta F = F_{-ATP} - F_{+ATP}$).

(j) (*Top*) NBD fluorescence intensity in the absence ($F_{\infty,-ATP}$) or presence ($F_{\infty,+ATP}$) of ATP is linear as a function of GlpG concentration after the degradation reaction was completed. $F_{\infty,-ATP}$ or $F_{\infty,+ATP}$ at each protein concentration was obtained by averaging the intensities in a time range when the fluorescence intensity reached a plateau. (*Bottom*) The net intensity change ($\Delta F_{\infty} = F_{\infty,-ATP} - F_{\infty,+ATP}$) is linear as a function of GlpG concentration. The slope of the intensity vs GlpG concentration plot yields the intensity change (ΔF_{∞}) per μ M GlpG degraded.

(k) The slope of fitted line in the early time range ($\Delta F/\text{min}$) is related to the initial rate of GlpG degradation by the relationship, the initial degradation rate ($\mu\text{M}/\text{min}$) = ($\Delta F/\text{min}$)/($\Delta F_{\infty}/\mu\text{M}$ degraded GlpG). This rate was further normalized by FtsH hexamer concentration ($[\text{FtsH}_6]$).

(l) The final plot of degradation rate vs GlpG concentration. Here the concentration of GlpG was expressed as a mole fraction of GlpG out of the total concentration of bicellar constituents, *i.e.*, $X_{\text{GlpG}} = [\text{GlpG}]/([\text{GlpG}]+[\text{DMPC}]+[\text{DMPG}]+[\text{CHAPS}]+[\text{FtsH}])$. This plot was used for enzyme kinetic analysis using Michaelis-Menten and Hill equations.

a

$$k_{U,app} = \frac{k_U k_{on} [mSA]}{k_F + k_{on} [mSA]}$$

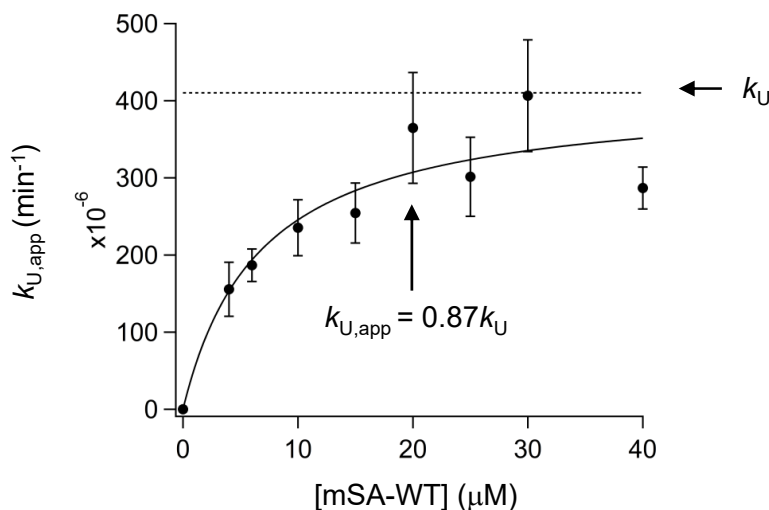
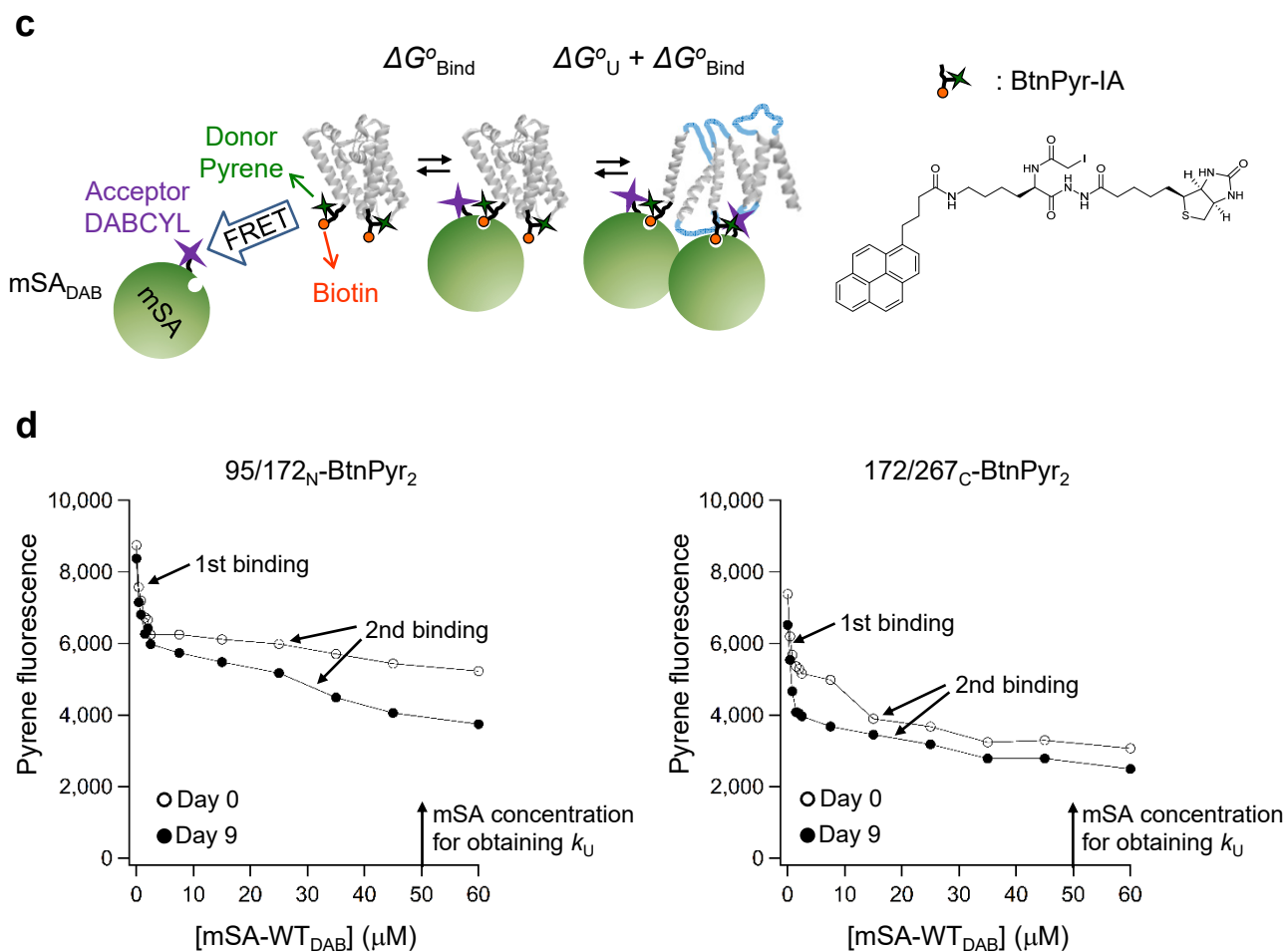
b

Figure S5, Related to Figures 4 and 5. Steric trapping of GlpG to measure the spontaneous unfolding rate k_U .

(a) Steric trapping for measuring k_U was achieved by shifting the reaction flux towards the unfolding direction using wild type monovalent streptavidin (mSA-WT) possessing high-affinity to biotin (mSA-WT; $K_{d,biotin} \approx 10^{-14}$ M; $k_{on,biotin} \approx 10^7$ M⁻¹ s⁻¹; $k_{off,biotin} \approx$ weeks).^{4,6} Under the steady state condition, in which k_U (unfolding rate) $\ll k_F$ (folding rate) and $k_{off,biotin} \ll k_{on,biotin} \cdot [mSA-WT]$ (on-rate of mSA to biotin), the apparent unfolding rate ($k_{U,app}$) can be approximated to an asymptotic equation shown in **Figure S5b**. At high mSA-WT concentration, $k_{U,app}$ approaches k_U .

(b) Dependence of the apparent unfolding rate ($k_{U,app}$) on the concentration of mSA-WT. The unfolding rates were measured for the double-biotin variant of GlpG, 95/172_N-BtnPyr₂ (1 μM, BtnPyr is described in **Figure S5c**) at different mSA concentrations in 20 mM sodium phosphate (pH 7.5), 200 mM NaCl and 5 mM dodecylmaltoside (DDM). GlpG activity was used as an unfolding readout in the unfolding kinetic measurement at each mSA-WT concentration (see also **Figure S2a**). The data were fit to the steady-state kinetic equation shown in **Figure S5a**. In the subsequent unfolding kinetic study (**Figures 4 and 5**), the mSA-to-GlpG molar ratio of 20 was used, at which $k_{U,app}$ was close to k_U (upward arrow). Errors designate \pm STD from fitting.



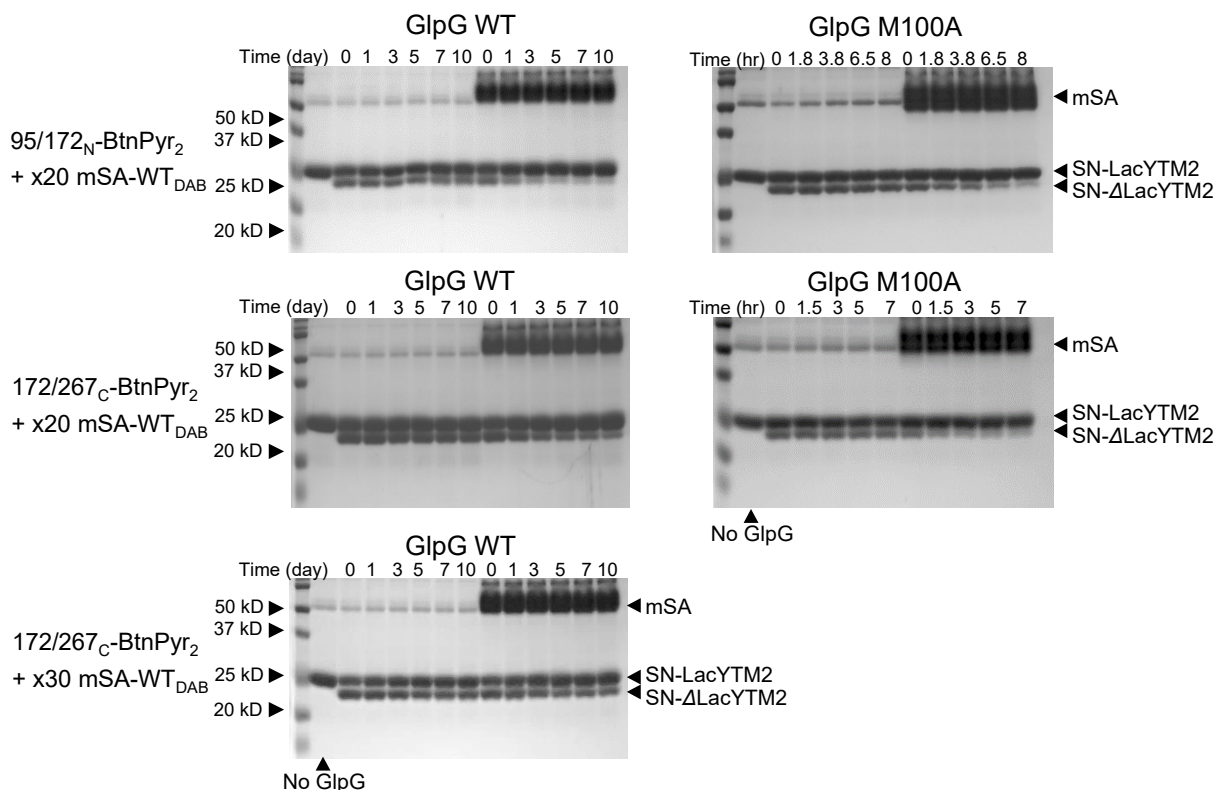
(Continued) Figure S5, Related to Figures 4 and 5. Steric trapping of GlpG to measure the spontaneous unfolding rate k_U .

(c-d) Unfolding in bicelles (**Figure 4b**) is caused by double-binding of mSA to GlpG due to steric trapping.

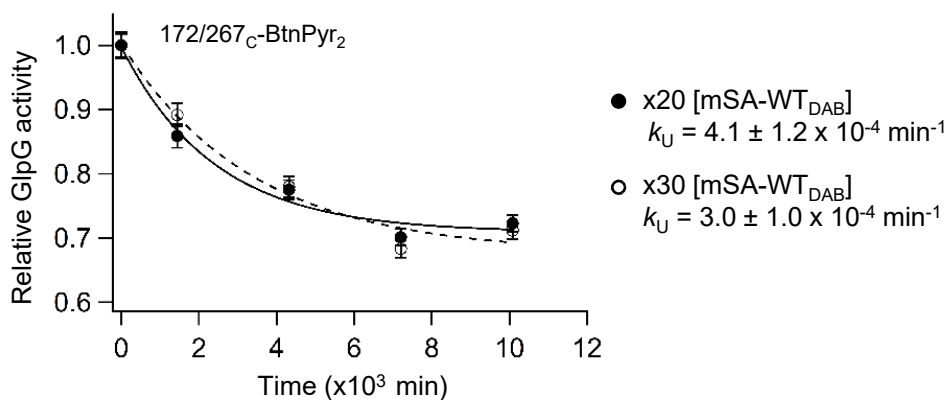
(c) Throughout this study, we used the thiol-reactive biotin derivative with a fluorescent pyrene group (BtPyr-iodoacetamide) and the single-cysteine variant of mSA (S83C) conjugated to nonfluorescent quencher dabcyl (mSA-WT_{DAB})¹. Thus, the designation of “biotin” in the main text is equivalent to BtPyr, and the designation of “mSA-WT” is equivalent to mSA-WT_{DAB}. This strategy enables sensitive detection of mSA binding to the biotin label by FRET (donor: pyrene; acceptor: dabcyl).

(d) Binding isotherm between a double-biotin GlpG variant (95/172_N or 172/267_C, 2.5 μM) and mSA-WT_{DAB} in DMPC/DMPG/CHAPS bicelles, 20 mM HEPES (pH 7.5) and 100 mM NaCl. The unhindered first binding is tight (1st binding) while the second binding coupled with unfolding is weak (2nd binding). The 2nd binding phase was slowly developed as the population of the trapped unfolded state increased over time (Day 0 vs Day 9). In the unfolding kinetic assay (**Figure 4b**) for measuring the spontaneous unfolding rate (k_U), the [mSA]/[GlpG] ratio of 20 (upward arrows) was used to ensure double binding of mSA to the double-biotin variants of GlpG.

e



f



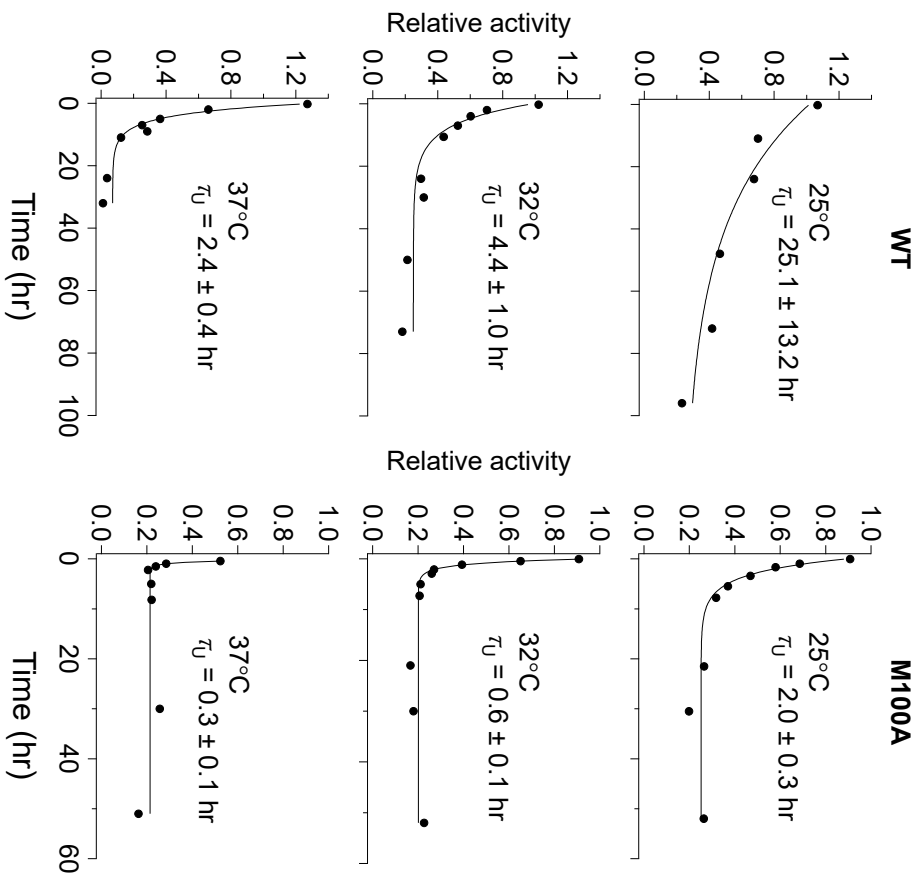
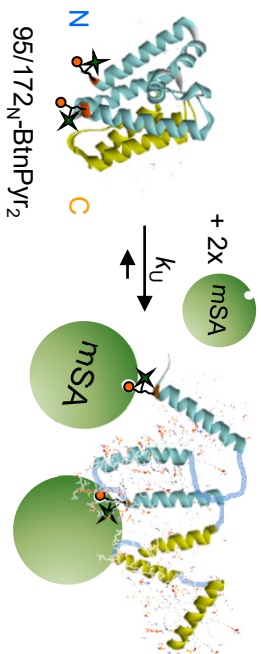
(Continued) **Figure S5, Related to Figures 4 and 5. Steric trapping of GlpG to measure the spontaneous unfolding rate k_U .**

(e) The spontaneous unfolding rates of GlpG (*left*) WT and (*right*) M100A variant (2.5 μM for each) were determined by steric trapping using GlpG activity as an unfolding readout. GlpG was incubated in the absence or presence of 50 μM mSA-WT at 37°C in 3% DMPC/DMPG/CHAPS bicelles, 40 mM HEPES (pH 7.5) and 100 mM NaCl. Steric trapping was carried out for both double-biotin variants, (*top*) 95/172_N-BtnPyr₂ and (*middle*) 172/267_C-BtnPyr₂ at a 20-times molar excess of [mSA-WT_{DAB}], and (*bottom*) 172/267_C-BtnPyr₂ at a 30-times molar excess of [mSA-WT_{DAB}]. The apparent unfolding rate ($k_{U,\text{app}}$) was determined by applying the first-order reaction kinetics. GlpG activity was measured by quantifying the amount of cleavage product of the model substrate SN-LacYTM2 on SDS-PAGE (see **Supporting Methods** for detailed experimental procedures).

(f) Comparison of the unfolding rates measured at 20-times and 30-times molar excess of mSA-WT_{DAB}. $k_{U,\text{app}}$'s obtained at a different molar excess of mSA-WT_{DAB} agreed reasonably well indicating that $k_{U,\text{app}}$'s that we determined (**Figure 4b**) are close to k_U . Errors designate \pm STD from fitting.

a

Global unfolding induced by steric trapping at the N-terminal biotin pair

**b**

Subglobal unfolding induced by steric trapping at the C-terminal biotin pair

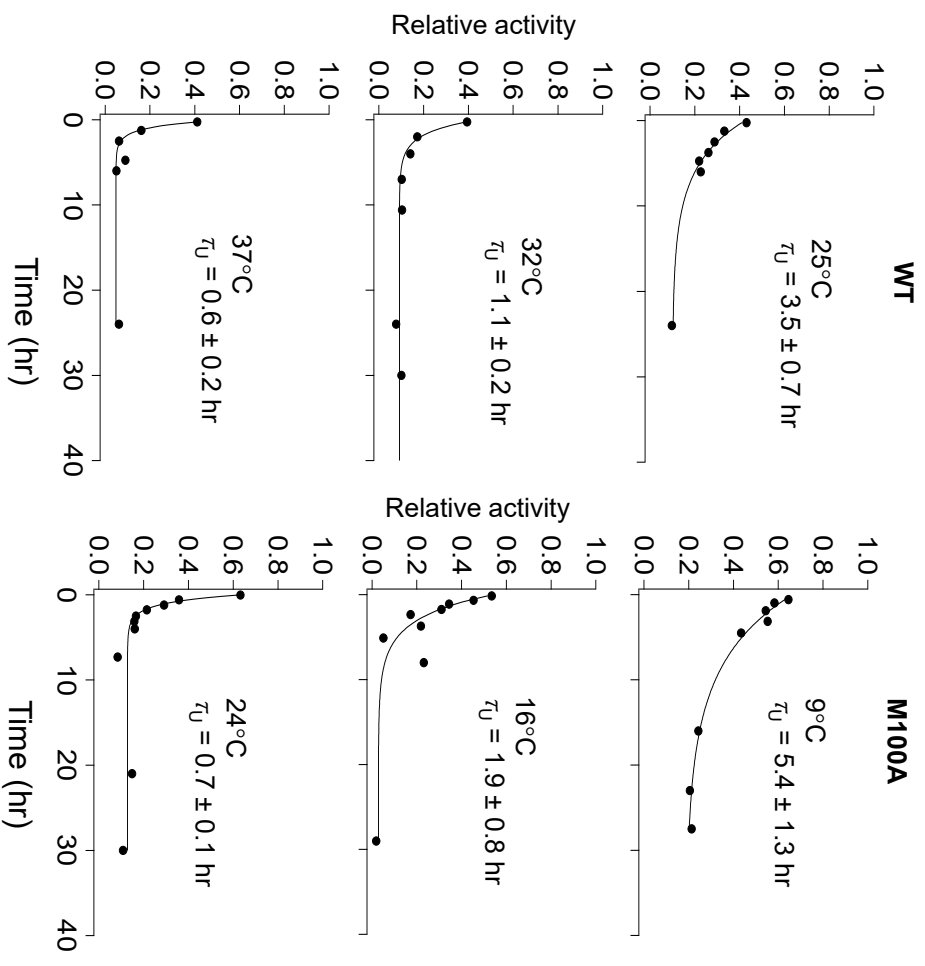
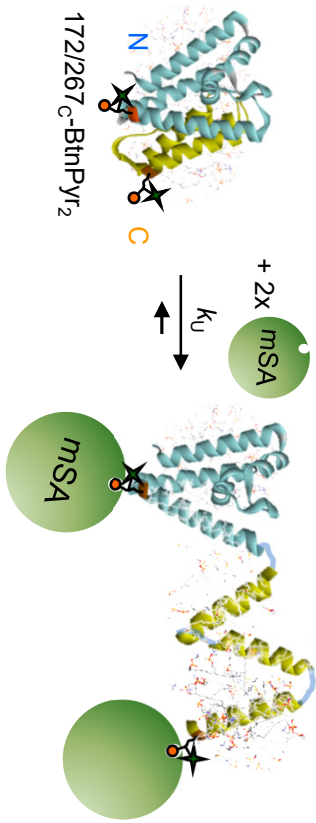


Figure S6, Related Figure 5. Unfolding energy landscape of GlpG in DDM micelles revealed by steric trapping.

Temperature-dependence of the unfolding kinetics (unfolding lifetime, $\tau_U = 1/k_U$) of GlpG WT and M100A variant in DDM micelles.

(a) GlpG unfolding was induced by steric trapping at the biotin labels located at the N-subdomain of GlpG (95/172_N-BtnPyr₂). Unfolding of the subdomain leads to global unfolding¹. Unfolding of GlpG (1 μ M) was measured by monitoring activity of GlpG cleaving the TM model substrate SN-LacYTM2 upon addition of excess mSA-WT (20 μ M) (see **Figure S5b**).

(b) Unfolding was induced by steric trapping at the biotin labels located at the C-subdomain of GlpG (172/267_N-BtnPyr₂). Unfolding of the C-subdomain leads to subglobal unfolding¹. Unfolding of GlpG (1 μ M) was measured by monitoring activity of GlpG cleaving SN-LacYTM2 upon addition of mSA-WT (20 μ M).

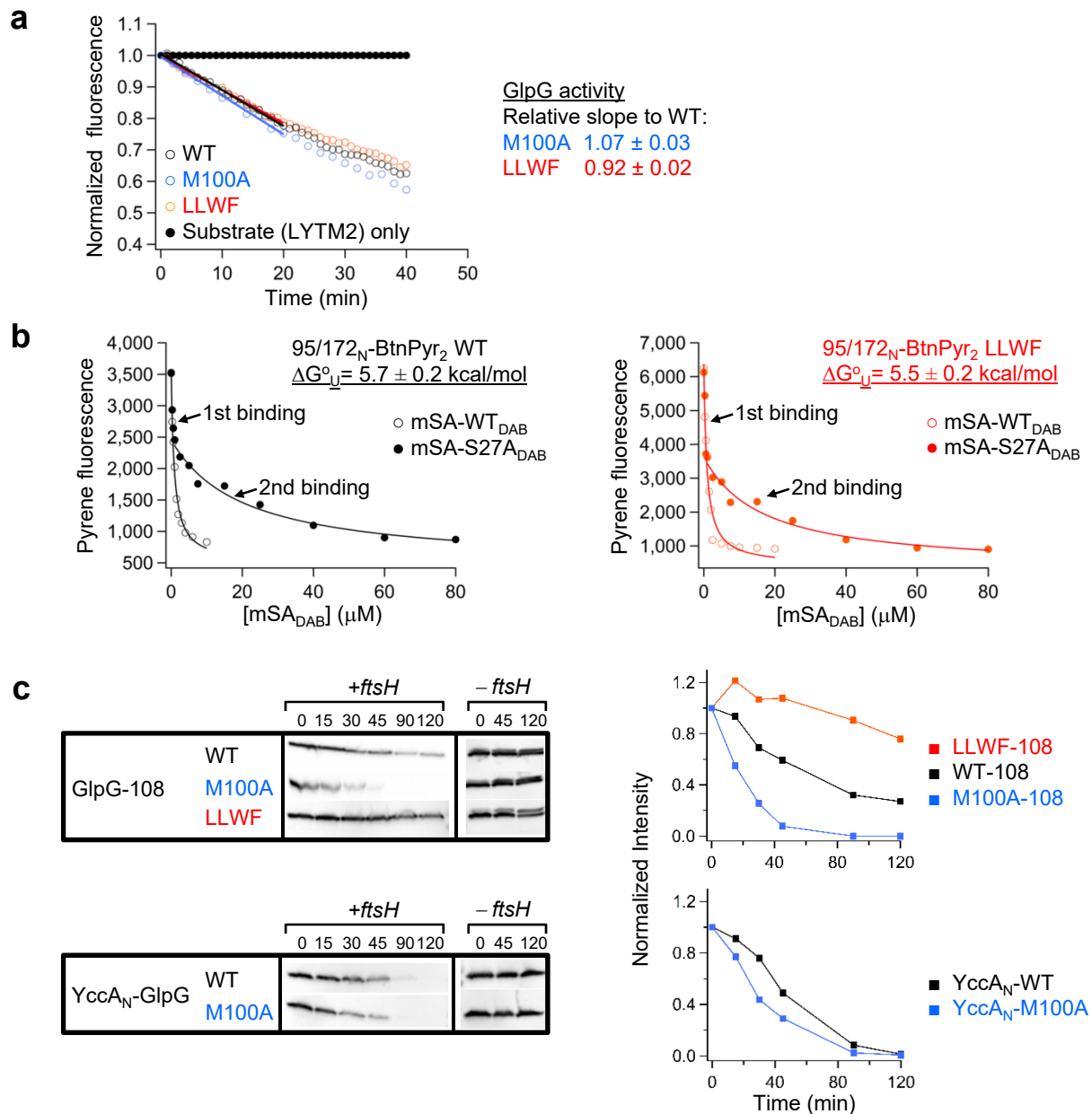


Figure S7, Related Figure 5. Characterization of M100A and LLWF variants.

(a) Comparison of activity of GlpG WT, M100A and LLWF variants. Proteolytic activity was measured by a fluorescence-based assay¹ using NBD-labeled SNLacYTM2 (10 μM) as a substrate in the presence of 1 μM GlpG in 20 mM HEPES (pH7.5), 100 mM NaCl, 0.5 mM TCEP and 5 mM DDM (see **Figure S2a**). The initial slope of each trace is directly related to the activity.

(b) Comparison of thermodynamic stability (ΔG°_U) of GlpG WT (95/172_N-BtnPyr₂) and its LLWF variant measured by steric trapping in 5 mM DDM. Detailed description of the steric trapping principle for measuring GlpG stability is described in **Figure S5c** and the literature¹. Briefly, the binding isotherm was obtained using weaker mSA variant mSA-S27A ($K_{d, \text{biotin}} = 1.4$ nM) labeled with dabcy1 quencher (mSA-S27A_{DAB}). The degree of attenuation of the second mSA binding phase relative to the first binding is correlated with the stability.

(c) Comparison of degradation of GlpG WT, M100A and LLWF variants *in vivo* measured by Western blotting. The intensities of GlpG bands were quantified using the ImageJ program.

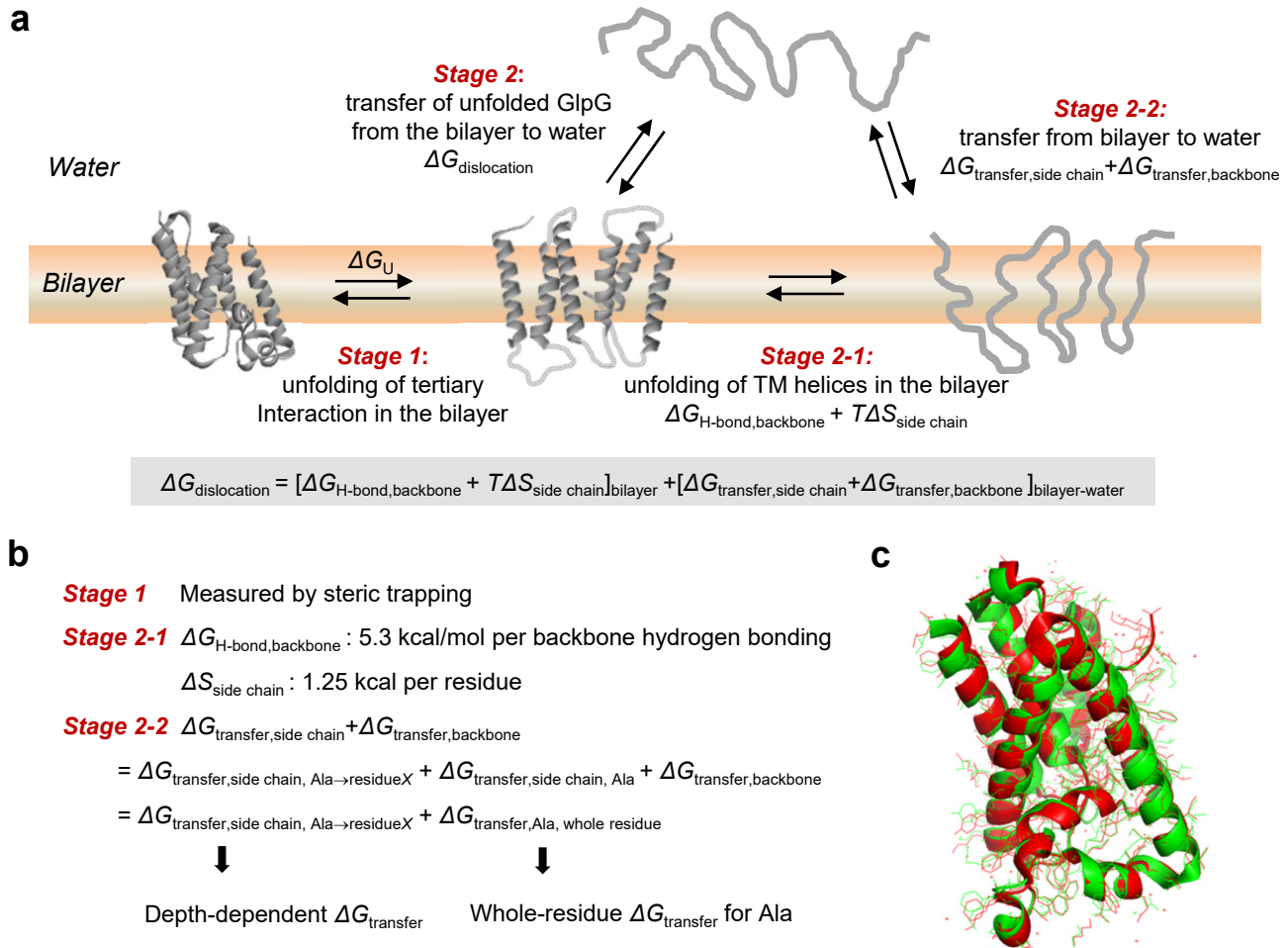


Figure S8, Related to Figures 5 and 6. Calculation of the free energy of dislocation ($\Delta G_{\text{dislocation}}$) using the depth-dependent hydrophobicity scale.

(a-b) Dissection of thermodynamics of FtsH-mediated degradation of helical membrane proteins.

(a) Overall, degradation of an helical membrane protein can be divided into two ATP-driven steps, unfolding of tertiary interactions within the bilayer (*Stage 1*) and dislocation of the unfolded state from the bilayer to the aqueous phase for proteolysis (*Stage 2*) (see also **Figure 6**). *Stage 2* can be further decomposed into *Stage 2-1* (backbone unfolding of TM helices in the bilayer) and *Stage 2-2* (transfer of fully unfolded GlpG from the bilayer to water) for thermodynamic analysis of dislocation free energy ($\Delta G_{\text{dislocation}}$).

(b) Thermodynamic stability in *Stage 1* can be experimentally determined using steric trapping. In *Stage 2-1*, the free energy change (5.3 kcal/mol) for breaking a backbone hydrogen bond (NH – CO) within the nonpolar hydrocarbon phase ($\Delta G_{\text{H-bond,backbone}}$) was obtained from the rigorous computational study using the density-functional theory.⁷ This value falls into the range of experimentally determined $\Delta G_{\text{H-bond,backbone}}$ (4–8 kcal/mol).³⁰ The average side-chain entropy change (1.25 kcal/mol) per residue ($T\Delta S_{\text{side chain}}$) was obtained from the study by Privalov.⁸ In *Stage 2-2*, the membrane depth-dependent transfer free energy change of a certain residue (X) relative to Ala ($\Delta G_{\text{transfer,side chain, Ala} \rightarrow \text{residue X}}$) was predicted using the computational method.^{11,12,13} The transfer free energy of the whole Ala residue including a peptide group ($\Delta G_{\text{transfer,Ala, whole residue}} = 0.16$ kcal/mol) was obtained from the knowledge-based unified hydrophobicity scale.⁹ Here it was assumed that the depth-dependence of $\Delta G_{\text{H-bond,backbone}}$ and $\Delta G_{\text{transfer,Ala, whole residue}}$ was not significant.¹⁰ The total $\Delta G_{\text{dislocation}}$ of all TM residues are shown in **Table S4**.

(c) Structural comparison of inhibitor-bound GlpG (2XOW) and apo-GlpG (3B45). The structure of inhibitor-bound GlpG was used to obtain the depth of each side chain in the TM helices using the OPM database because the apo-structure was not included in the database¹⁴. The two structures are highly similar (RMSD = 0.6 Å).

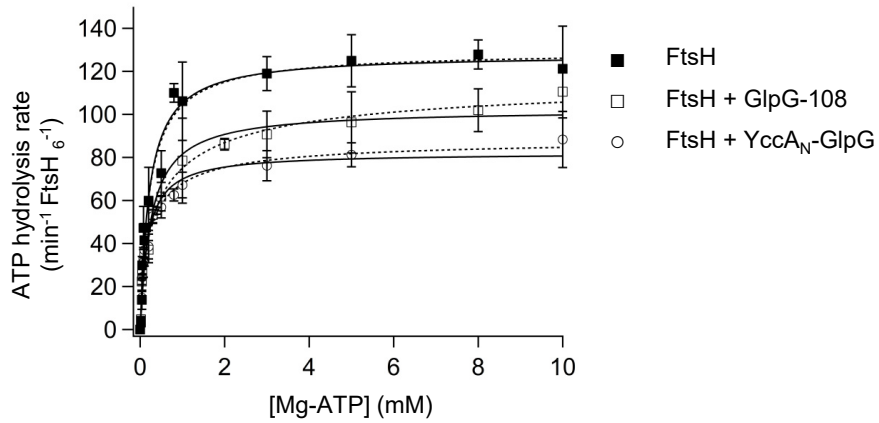


Figure S9. ATPase activity of FtsH in the presence of bound substrate.

ATPase activity of FtsH was measured in the presence of saturating concentrations of the membrane protein substrate GlpG-108 and YccA_N-GlpG. ATP hydrolysis by FtsH (2 μM) was measured in DMPC/DMPG/CHAPS bicelles at 37°C using the enzyme-coupled assay. Data are represented as mean ± SEM ($n = 3$). See **Table S5** for fitted kinetic parameters.

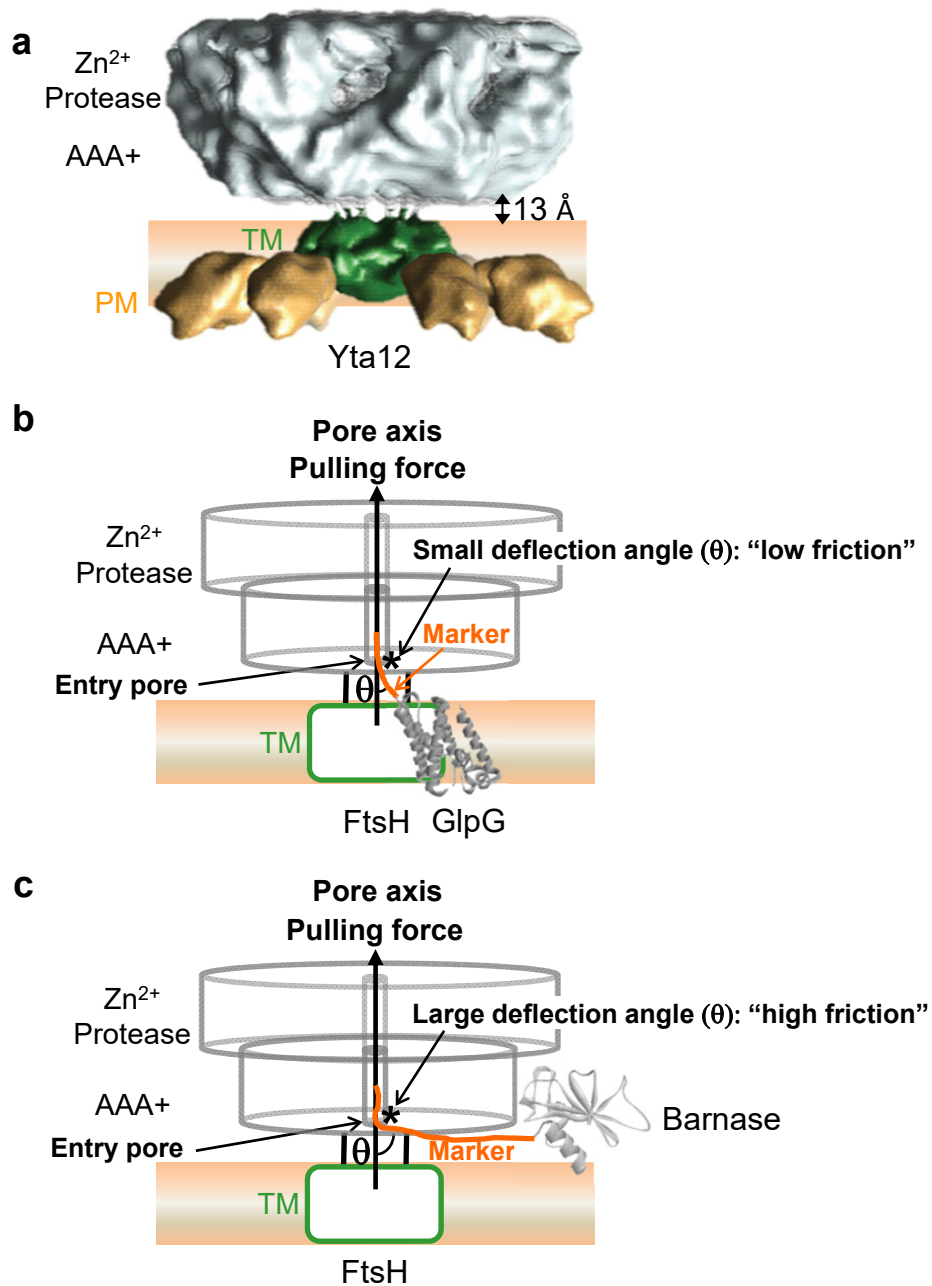


Figure S10. A mechanical model to explain why FtsH more efficiently degrades membrane proteins than water-soluble proteins.

(a) Cryo-electron microscopy image of an FtsH-ortholog Yta12 of yeast showing a narrow 13 Å gap between the AAA+ hexamer and the membrane³⁷.

(b) When a membrane-protein (GlpG here) with a flexible tail as a degradation marker binds to FtsH, the bound tail will align the TM helices of GlpG at a small deflection angle³⁸ relative to the direction of the pulling force. In this case, less frictional force is generated at the deflection point (*) near the substrate entry pore and the pulling forces will be efficiently applied to the membrane protein. Despite the presence of the PM (periplasmic) domain, probably GlpG can approach close to the pore axis because of the large gap between neighboring PM domains.

(c) When a water-soluble protein (barnase here) with a flexible tail binds to FtsH, the bound tail aligns barnase at a large deflection angle ($\sim 90^\circ$) relative to the direction of the pulling force. In this case, more frictional force is exerted at the deflection point, reducing the effective pulling force.

REFERENCES FOR SUPPORTING INFORMATION

- (1) Guo, R., Gaffney, K., Yang, Z., Kim, M., Sungsuwan, S., Huang, X., Hubbell, W. L., and Hong, H., Steric trapping reveals a cooperativity network in the intramembrane protease GlpG. *Nat Chem Biol* **2016**, *12* (5), 353-360.
- (2) Baker, R. P. and Urban, S., Architectural and thermodynamic principles underlying intramembrane protease function. *Nat Chem Biol* **2012**, *8* (9), 759-768.
- (3) Ogura, T., Inoue, K., Tatsuta, T., Suzaki, T., Karata, K., Young, K., Su, L. H., Fierke, C. A., Jackman, J. E., Raetz, C. R. H., Coleman, J., Tomoyasu, T., and Matsuzawa, H., Balanced biosynthesis of major membrane components through regulated degradation of the committed enzyme of lipid A biosynthesis by the AAA protease FtsH (HflB) in *Escherichia coli*. *Mol Microbiol* **1999**, *31* (3), 833-844.
- (4) Howarth, M., Chinnapen, D. J., Gerrow, K., Dorrestein, P. C., Grandy, M. R., Kelleher, N. L., El-Husseini, A., and Ting, A. Y., A monovalent streptavidin with a single femtomolar biotin binding site. *Nat Methods* **2006**, *3* (4), 267-273.
- (5) Jefferson, R. E., Blois, T. M., and Bowie, J. U., Membrane proteins can have high kinetic stability. *J Am Chem Soc* **2013**, *135* (40), 15183-15190.
- (6) Srisa-Art, M., Dyson, E. C., deMello, A. J., and Edel, J. B., Monitoring of real-time streptavidin-biotin binding kinetics using droplet microfluidics. *Anal Chem* **2008**, *80* (18), 7063-7067.
- (7) BenTal, N., Sitkoff, D., Topol, I. A., Yang, A. S., Burt, S. K., and Honig, B., Free energy of amide hydrogen bond formation in vacuum, in water, and in liquid alkane solution. *J Phys Chem B* **1997**, *101* (3), 450-457.
- (8) Privalov, P. L., Stability of proteins: small globular proteins. *Adv Protein Chem* **1979**, *33*, 167-241.
- (9) Koehler, J., Woetzel, N., Staritzbichler, R., Sanders, C. R., and Meiler, J., A unified hydrophobicity scale for multispan membrane proteins. *Proteins* **2009**, *76* (1), 13-29.
- (10) Hessa, T., Meindl-Beinker, N. M., Bernsel, A., Kim, H., Sato, Y., Lerch-Bader, M., Nilsson, I., White, S. H., and von Heijne, G., Molecular code for transmembrane-helix recognition by the Sec61 translocon. *Nature* **2007**, *450* (7172), 1026-1030.
- (11) Tian, W., Naveed, H., Lin, M., and Liang, J., GeTFEP: a general transfer free energy profile for transmembrane proteins. *BioRxiv* **2017**, 191650.
- (12) Lin, M., Gessmann, D., Naveed, H., and Liang, J., Outer membrane protein folding and topology from a computational transfer free energy scale. *J Am Chem Soc* **2016**, *138* (8), 2592-2601.

- (13) Tian, W., Lin, M., Naveed, H., and Liang, J., Efficient computation of transfer free energies of amino acids in beta-barrel membrane proteins. *Bioinformatics* **2017**, *33* (11), 1664-1671.
- (14) Lomize, M. A., Lomize, A. L., Pogozheva, I. D., and Mosberg, H. I., OPM: orientations of proteins in membranes database. *Bioinformatics* **2006**, *22* (5), 623-625.
- (15) Iwakura, M., Nakamura, T., Yamane, C., and Maki, K., Systematic circular permutation of an entire protein reveals essential folding elements. *Nat Struct Biol* **2000**, *7* (7), 580-585.
- (16) Touchette, N. A., Perry, K. M., and Matthews, C. R., Folding of dihydrofolate reductase from *Escherichia coli*. *Biochemistry* **1986**, *25* (19), 5445-5452.
- (17) Tian, J., Woodard, J. C., Whitney, A., and Shakhnovich, E. I., Thermal stabilization of dihydrofolate reductase using monte carlo unfolding simulations and its functional consequences. *PLoS Comput Biol* **2015**, *11* (4), e1004207.
- (18) Kim, Y. I., Burton, R. E., Burton, B. M., Sauer, R. T., and Baker, T. A., Dynamics of substrate denaturation and translocation by the ClpXP degradation machine. *Mol Cell* **2000**, *5* (4), 639-648.
- (19) Nicholls, S. B. and Hardy, J. A., Structural basis of fluorescence quenching in caspase activatable-GFP. *Protein Sci* **2013**, *22* (3), 247-257.
- (20) Clarke, J. and Fersht, A. R., Engineered disulfide bonds as probes of the folding pathway of barnase: increasing the stability of proteins against the rate of denaturation. *Biochemistry* **1993**, *32* (16), 4322-4329.
- (21) Fersht, A. R., A kinetically significant intermediate in the folding of barnase. *Proc Natl Acad Sci U S A* **2000**, *97* (26), 14121-14126.
- (22) Makarov, A. A., Protasevich, I., Lobachov, V. M., Kirpichnikov, M. P., Yakovlev, G. I., Gilli, R. M., Briand, C. M., and Hartley, R. W., Thermostability of the barnase-barstar complex. *FEBS Lett* **1994**, *354* (3), 251-254.
- (23) Waldburger, C. D., Schildbach, J. F., and Sauer, R. T., Are buried salt bridges important for protein stability and conformational specificity? *Nat Struct Biol* **1995**, *2* (2), 122-128.
- (24) Sauer, R. T., Milla, M. E., Waldburger, C. D., Brown, B. M., and Schildbach, J. F., Sequence determinants of folding and stability for the P22 Arc repressor dimer. *FASEB J* **1996**, *10* (1), 42-48.
- (25) Robinson, C. R., Rentzeperis, D., Silva, J. L., and Sauer, R. T., Formation of a denatured dimer limits the thermal stability of Arc repressor. *J Mol Biol* **1997**, *273* (3), 692-700.

- (26) Brennan, C. A., Christianson, K., La Fleur, M. A., and Mandeck, W., A molecular sensor system based on genetically engineered alkaline phosphatase. *Proc Natl Acad Sci U S A* **1995**, 92 (13), 5783-5787.
- (27) Lau, F. W. and Bowie, J. U., A method for assessing the stability of a membrane protein. *Biochemistry* **1997**, 36 (19), 5884-5892.
- (28) Zhou, Y. and Bowie, J. U., Building a thermostable membrane protein. *J Biol Chem* **2000**, 275 (10), 6975-6979.
- (29) Min, D., Jefferson, R. E., Bowie, J. U., and Yoon, T. Y., Mapping the energy landscape for second-stage folding of a single membrane protein. *Nat Chem Biol* **2015**, 11 (12), 981-987.
- (30) Cao, Z., Hutchison, J. M., Sanders, C. R., and Bowie, J. U., Backbone Hydrogen Bond Strengths Can Vary Widely in Transmembrane Helices. *J Am Chem Soc* **2017**, 139 (31), 10742-10749.
- (31) Okuno, T., Yamada-Inagawa, T., Karata, K., Yamanaka, K., and Ogura, T., Spectrometric analysis of degradation of a physiological substrate sigma32 by Escherichia coli AAA protease FtsH. *J Struct Biol* **2004**, 146 (1-2), 148-154.
- (32) Kenniston, J. A., Baker, T. A., Fernandez, J. M., and Sauer, R. T., Linkage between ATP consumption and mechanical unfolding during the protein processing reactions of an AAA(+) degradation machine. *Cell* **2003**, 114 (4), 511-520.
- (33) Hersch, G. L., Burton, R. E., Bolon, D. N., Baker, T. A., and Sauer, R. T., Asymmetric interactions of ATP with the AAA+ ClpX6 unfoldase: allosteric control of a protein machine. *Cell* **2005**, 121 (7), 1017-1027.
- (34) Gur, E. and Sauer, R. T., Recognition of misfolded proteins by Lon, a AAA(+) protease. *Genes Dev* **2008**, 22 (16), 2267-2277.
- (35) Wohlever, M. L., Nager, A. R., Baker, T. A., and Sauer, R. T., Engineering fluorescent protein substrates for the AAA+ Lon protease. *Protein Eng Des Sel* **2013**, 26 (4), 299-305.
- (36) Benaroudj, N. and Goldberg, A. L., PAN, the proteasome-activating nucleotidase from archaeobacteria, is a protein-unfolding molecular chaperone. *Nat Cell Biol* **2000**, 2 (11), 833-839.
- (37) Lee, S., Augustin, S., Tatsuta, T., Gerdes, F., Langer, T., and Tsai, F. T., Electron cryomicroscopy structure of a membrane-anchored mitochondrial AAA protease. *J Biol Chem* **2011**, 286 (6), 4404-4411.
- (38) Bowie, J. U., Helix packing in membrane proteins. *J Mol Biol* **1997**, 272 (5), 780-789.